Long-Baseline Neutrino Experiment (LBNE) Project

Conceptual Design Report

Volume 1: The LBNE Project

March 17, 2012

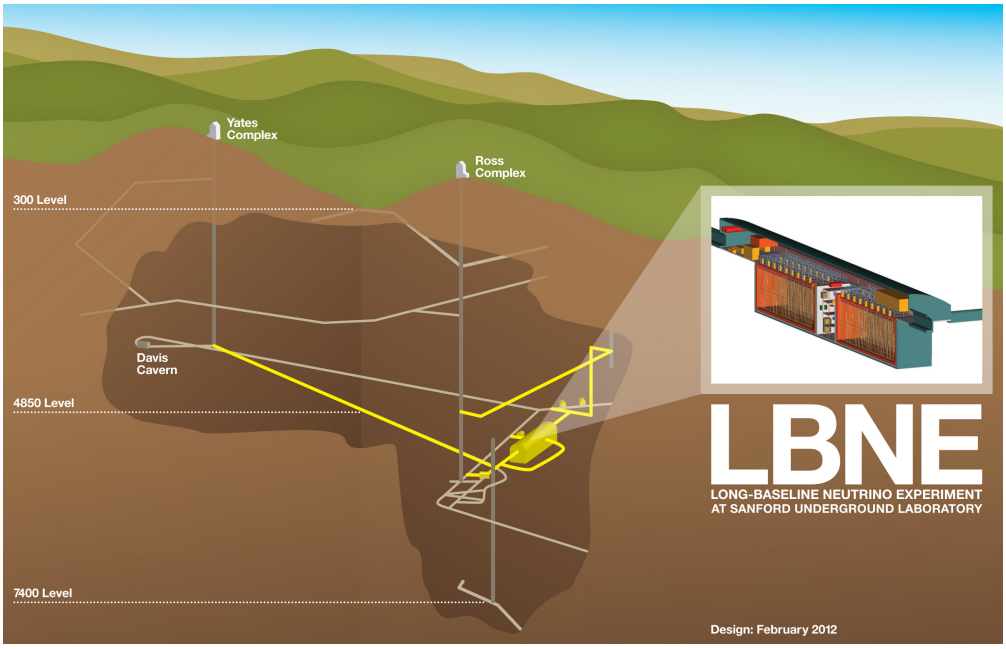

Contents

Acronyms, Abbreviations and Units

3D	3 dimensional, also 2D
ALICE	A Large Ion Collider Experiment (at CERN)
AoR	area of refuge
C.L.	confidence level
CC	charged current (interaction)
CCQE	charged current qusi-elastic (interaction)
CDR	Conceptual Design Report
CP	charge, parity
CPT	charge, parity, time
DAQ	data acquisition
DocDB	document database application used by LBNE and other Fermilab experiments
DOE	Department of Energy
DUSEL	Deep Underground Science and Engineering Laboratory
ESH	Environment, Safety and Health
eV	electron-Volt, unit of energy (also keV, MeV, GeV, etc.)
FGT	Fine-Grained Tracker
GENIE	Generates Events for Neutrino Interaction Experiments (an object-oriented neutrino Monte Carlo generator)
GUT	grand unified theory
ICARUS	Imaging Cosmic And Rare Underground Signals (experiment at LNGS)

L	level, indicates depth in feet underground at a site, e.g., 4850L
L/E	length to energy ratio
LAr-FD	LBNE's Liquid Argon Far Detector
LArTPC	liquid argon time projection chamber
LArTPCT	Liquid Argon Time Projection Chamber Tracker system
LBNE	Long-Baseline Neutrino Experiment
LNGS	Gran Sasso National Laboratory
MaVaNs	mass varying neutrinos
MI	Main Injector (at Fermilab)
NC	neutral current (interaction)
ND	(Near Site) neutrino detector
NDC	Near Detector Complex; refers to the subproject
NSI	nonstandard interactions
OHEP	Office of High Energy Physics
OPERA	Oscillation Project with Emulsion-Racking Apparatus experiment, at LNGS
POT	protons on target
QA	quality assurance
QE	quasi-elastic (interaction)
SDSTA	South Dakota Science and Technology Authority
SUSY	supersymmetry
T	ton, also Tesla
TPC	time projection chamber (not used as 'total project cost' in the CDR except in Section 4.3)
W	watt (also mW, kW, MW)
WBS	Work Breakdown Structure

List of Figures

List of Tables

1 About the LBNE Conceptual Design Report

The Long-Baseline Neutrino Experiment (LBNE) Project will provide facilities to enable a world-class program in neutrino physics that can measure fundamental physical parameters, explore physics beyond the Standard Model and better elucidate the nature of matter and anti-matter. Specifically, LBNE will build a new high-intensity neutrino beam at the Fermi National Accelerator Laboratory (Fermilab) aimed at the Sanford Underground Laboratory at Homestake (Sanford Laboratory), 1,300 km away, where it will build a massive neutrino detector. The experiment will be optimized for precision measurement of $\nu_\mu \rightarrow \nu_e$ oscillations with the goal of searching for CP-violation in the neutrino sector, as well as making other precision oscillation measurements. By placing the detector deep underground at Sanford Laboratory, LBNE will also be able to execute a rich program in proton decay, neutrino astrophysics and other non-accelerator physics.

The Long-Baseline Neutrino Experiment (LBNE) Conceptual Design Report (CDR) describes, at a conceptual level, the scope and design of the experimental and conventional facilities that the LBNE Project plans to build. In general terms, the scope comprises

- an intense neutrino beam aimed at a far site
- detectors located at the near site just downstream of the neutrino source
- a massive neutrino detector located at the far site
- construction of facilities at both the near and far sites

The selected near and far sites are Fermilab in Batavia, Illinois and the Sanford Laboratory in Lead, South Dakota, respectively.

This CDR is organized into six stand-alone volumes, one to describe the overall LBNE Project and one for each of its component subprojects:

1. The LBNE Project

2. The Beamline at the Near Site
3. Detectors at the Near Site
4. The Liquid Argon Detector at the Far Site
5. Conventional Facilities at the Near Site
6. Conventional Facilities at the Far Site

Volume 1 is intended to provide readers of varying backgrounds an introduction to LBNE and to the following volumes of this CDR. It contains high-level information and refers the reader to topic-specific volumes and supporting documents, as appropriate. This volume outlines the physics program that LBNE is designed to carry out. Readers desiring detailed information about the physics program and the experimental capabilities are referred to the Case Study Report (Liquid Argon TPC Detector) [2].

Each Volume 2 through 6 contains a common, brief introduction to the overall LBNE Project, an introduction to the individual subproject and a detailed description of its conceptual design.

A list of supporting documents providing information on risk analysis and mitigation, value engineering, costing, project management and other topics not directly in the design scope are listed in Chapter 7.

2 Executive Summary

2.1 Introduction to the LBNE Project

The Long-Baseline Neutrino Experiment (LBNE) Project team has prepared this Conceptual Design Report (CDR), which describes a world-class facility that will enable the scientific community to carry out a compelling research program in neutrino physics. The ultimate goal in the operation of the facility and experimental program is to measure fundamental physical parameters, explore physics beyond the Standard Model and better elucidate the nature of matter and antimatter.

2.1.1 Scientific Motivation

Although the Standard Model of particle physics presents a remarkably accurate description of the elementary particles and their interactions, it is known that the current model is incomplete and that a more fundamental underlying theory must exist. Results from the last decade, that the three known types of neutrinos have nonzero mass, mix with one another and oscillate between generations, implies physics beyond the Standard Model [3].

The three-flavor-mixing scenario for neutrinos can be described by three mixing angles (θ_{12}, θ_{23} and θ_{13}) and one CP-violating phase (δ_{CP}). The probability for neutrino oscillation also depends on the difference in the squares of the neutrino masses, $\Delta m^2_{ij} = m^2_i - m^2_j$; three neutrinos implies two independent mass-squared differences (Δm^2_{21} and Δm^2_{32}).

The entire complement of neutrino experiments to date has measured five of the mixing parameters: three angles, θ_{12}, θ_{23}, and recently θ_{13}, and two mass differences, Δm^2_{21} and Δm^2_{32}. The sign of Δm^2_{21} is known, but not that of Δm^2_{32}. The value of θ_{13} has been determined to be much smaller than the other two mixing angles [4], implying that mixing is quantitatively different in the neutrino and quark sectors.

Observations of $\nu_\mu \rightarrow \nu_e$ oscillations of a beam (composed initially of muon neutrinos, ν_μ) over a long baseline are the key to unambiguously determining the mass hierarchy (the sign of

Δm^2_{32}), and the unknown CP-violating phase δ_{cp}. The signature of CP violation is a difference in the probabilities for $\nu_\mu \to \nu_e$ and $\overline{\nu}_\mu \to \overline{\nu}_e$ transitions. The study of the disappearance of ν_μ probes θ_{23} and $|\Delta m^2_{32}|$. Non-standard physics can manifest itself in differences observed in higher precision measurements of ν_μ and $\bar{\nu}_\mu$ disappearance over long baselines. The precision with which we know the current set of neutrino-oscillation parameters ensures that the compelling physics program outlined for LBNE is feasible with the combination of baseline, detector mass and beam that is proposed.

2.1.2 LBNE and the U.S. Neutrino-Physics Program

In its 2008 report, the Particle Physics Project Prioritization Panel (P5) recommended a world-class neutrino-physics program as a core component of the U.S. particle-physics program [5]. Included in the report is the long-term vision of a large detector in the Sanford Underground Laboratory in Lead, S.D., the site of the formerly proposed Deep Underground Science and Engineering Laboratory (DUSEL), and a high-intensity neutrino source at Fermilab.

On January 8, 2010, the Department of Energy approved the Mission Need for a new long-baseline neutrino experiment that would enable this world-class program and firmly establish the U.S. as the leader in neutrino science. The LBNE Project is designed to meet this Mission Need.

With the facilities provided by the LBNE Project and the unique features of the experiment – in particular the long baseline, the broad-band beam and the high resolution of the detector – the LBNE Science Collaboration proposes to mount a broad attack on the science of neutrinos with sensitivity to all known parameters in a single experiment. The focus of the program will be the explicit demonstration of leptonic CP violation, if it exists, by precisely measuring the asymmetric oscillations of muon-type neutrinos and antineutrinos into electron-type neutrinos and antineutrinos.

The experiment will enable the most precise measurements of the neutrino oscillation parameters, in particular, the CP-violating phase in the three-flavor framework, and the search for new physics that would show up as deviations from this model.

A configuration of the LBNE facility, in which a large neutrino detector is located deep underground, could also provide opportunities for research in other areas of physics, such as nucleon decay and neutrino astrophysics, including studies of neutrino bursts from locally occurring supernovae. The scientific goals and capabilities of LBNE are summarized in Chapter 6 and fully described in the LBNE Case Study report for a Liquid Argon Time Projection Chamber (LArTPC) [2] and the 2010 Interim Report of the Long-Baseline Neutrino Experiment Collaboration Physics Working Groups [6].

2.1.3 Overview of Project Organization

The LBNE Project Office at Fermilab is headed by the Project Manager and assisted by the Project Engineer, Project Systems Engineer and Project Scientist. Project Office support staff include a Project Controls Manager and supporting staff, a Financial Manager, an ES&H Manager, a Computing Coordinator, Quality Assurance and Risk Managers, a documentation team and administrative support. The construction of LBNE is supported by the laboratories and universities of the LBNE Science Collaboration, which provides scientific, engineering and technical expertise. More information on Project organization can be found in Chapter 4, and a full description of LBNE Project management is contained in The LBNE Project Management Plan [7].

2.2 Overview of the LBNE Science Objectives

The primary science objectives of the LBNE Project are the following experiments [8]:

1. Search for, and precision measurements of, the parameters that govern $\nu_\mu \rightarrow \nu_e$ oscillations. This includes precision measurement of the third mixing angle, θ_{13}, and the CP-violating phase δ_{CP} and determination of the mass ordering (the sign of Δm^2_{32}).
2. Precision measurements of θ_{23} and $|\Delta m^2_{32}|$ in the ν_μ and $\bar{\nu}_\mu$ disappearance channel.
3. Search for proton decay, yielding measurement of the partial lifetime of the proton (τ/BR) in one or more important candidate decay modes, e.g. $p \rightarrow e^+\pi^0$ or $p \rightarrow K^+\nu$, or significant improvement in limits on it.
4. Detection and measurement of the neutrino flux from a core-collapse supernova within our galaxy, should one occur during the lifetime of LBNE.

A high-level discussion of these objectives as well as a list of additional objectives that LBNE may pursue can be found in Chapter 3. The topics are covered thoroughly in the LBNE Case Study Report (Liquid Argon TPC Far Detector) [2] and the 2010 Interim Report of the Long-Baseline Neutrino Experiment Collaboration Physics Working Groups [6].

2.3 Principal Parameters of the LBNE Project

The individual CDR volumes provide detail on the designs that LBNE has developed, based on a carefully constructed set of requirements that are organized in a traceable flow-down structure. Scientific requirements for LBNE, provided by the LBNE Collaboration, follow

from the science objectives. Design of individual subprojects, systems and components are based on mid- and low-level requirements, respectively, that trace all the way back either to the science requirements or to LBNE's set of high-level programmatic requirements.

The experimental capabilities and performance of the Far Detector technology is documented thoroughly in the LBNE Case Study Report for a Liquid Argon TPC [9] and summarized in Chapter 6.

Table 2–1 summarizes the principal parameters of the experiment.

Table 2–1: LBNE Principal Parameters

Project Element Parameter	Value
Near- to Far-Site Baseline	1,300 km
Primary Proton Beam Power	708 kW, upgradable to 2.3 MW
Protons on Target per Year	6.5×10^{20}
Primary Beam Energy	60 – 120 GeV (tunable)
Neutrino Beam Type	Horn-focused with decay volume
Neutrino Beam Energy Range	0.5 – 5 GeV
Neutrino Beam Decay Pipe Diameter × Length	4 m × 200 m
Near Site Neutrino Detector Type	Liquid Argon Time Projection Chamber (LArTPC) Tracker
Near Site Neutrino Detector Active Mass	18 tons
Far Detector Type	LArTPC
Far Detector Active (Fiducial) Mass	40 (33) ktons
Far Detector Depth	1480 m

3 LBNE Science Objectives

The LBNE science objectives are divided into three categories: *primary*, *secondary* and *additional secondary*. Our conceptual design by definition addresses the primary objectives. Secondary objectives are defined as those that may be enabled by the facility designed to achieve the primary objectives, i.e. with little or no impact on the cost or schedule. Achievement of the additional secondary objectives, in contrast, may require future upgrades to the facility designed to achieve the primary objectives.

The priorities for the scientific research to be enabled by the LBNE Project follow from the P5 recommendations, the Department of Energy (DOE) Mission Need Statement, discussions with the DOE Office of High Energy Physics (OHEP), Fermilab management and the LBNE Science Collaboration.

The primary mission of the LBNE Project is to construct facilities that will enable observation of $\nu_\mu \rightarrow \nu_e$ appearance over a distance (baseline) of greater than 1,000 km. At the LBNE baseline of 1,300 km, the magnitude of this signal is governed by the neutrino mass differences, the mass ordering, the CP-violating phase δ_{cp}, and all three mixing angles θ_{12}, θ_{23} and θ_{13}. The various oscillation parameters impact the appearance spectrum differently at different neutrino energies and for neutrinos versus anti-neutrinos. Therefore, precise measurement of $\nu_\mu \rightarrow \nu_e$ and $\bar{\nu}_\mu \rightarrow \bar{\nu}_e$ oscillations over a wide range of neutrino energies would allow for unambiguous determination of the neutrino mass ordering and mass differences, as well as precision measurements of δ_{cp} and all three mixing angles. Measurement of this neutrino-oscillation channel would also allow for research into CP violation in the neutrino sector, which may be connected to the dominance of matter over antimatter in the universe.

The entire set of LBNE science objectives is listed below.

1. Primary
   (a) Search for, and precision measurements of, the parameters that govern $\nu_\mu \rightarrow \nu_e$ oscillations, as discussed above; this includes precision measurements of the third mixing angle, θ_{13}, measurement of the CP violating phase δ_{CP} and determination of the mass ordering (the sign of Δm^2_{32})

(b) Precision measurements of θ_{23} and $|\Delta m^2_{32}|$ in the ν_μ-disappearance channel

(c) Search for proton decay, yielding measurement of the partial lifetime of the proton (τ/BR) in one or more important candidate decay modes, e.g. $p \to e^+\pi^0$ or $p \to K^+\nu$, or significant improvement in limits on it

(d) Detection and measurement of the neutrino flux from a core-collapse supernova within our galaxy, should one occur during the lifetime of LBNE

2. Secondary

(a) Other accelerator-based neutrino-oscillation measurements

(b) Measurements of neutrino-oscillation phenomena using atmospheric neutrinos

(c) Measurements of neutrino-oscillation phenomena and of solar physics using solar neutrinos

(d) Measurement of other astrophysical phenomena using medium-energy neutrinos

(e) Near detector studies of neutrino interactions

(f) Near detector studies of nuclear and nucleon structure

(g) Near detector searches for new physics

3. Additional secondary

(a) Detection and measurement of the diffuse supernova-neutrino flux

(b) Measurements of astrophysical and geophysical neutrinos of low energy

4 Project Organization

4.1 Overview

The LBNE Project consists of a set of subprojects, coordinated by a central Project Office located at Fermilab:

1. Project Management
2. Beamline
3. Near Detector Complex
4. (Water Cherenkov Far Detector – excluded as a Far Detector technology for LBNE in January 2012)
5. Liquid Argon Far Detector
6. Conventional Facilities

The LBNE Project Office at Fermilab is headed by the Project Manager and assisted by the Project Engineer and Project Scientist. Project Office support staff include a Project Controls Manager and supporting staff, a Financial Manager, a Manager for Environment, Safety and Health (ES&H), a Computing Coordinator, Quality Assurance (QA) and Risk Managers, a documentation team and administrative support.

The construction of LBNE is supported by the laboratories and universities of the LBNE Science Collaboration, which provides scientific, engineering and technical expertise. A Project organization chart is shown in Figure 4–1.

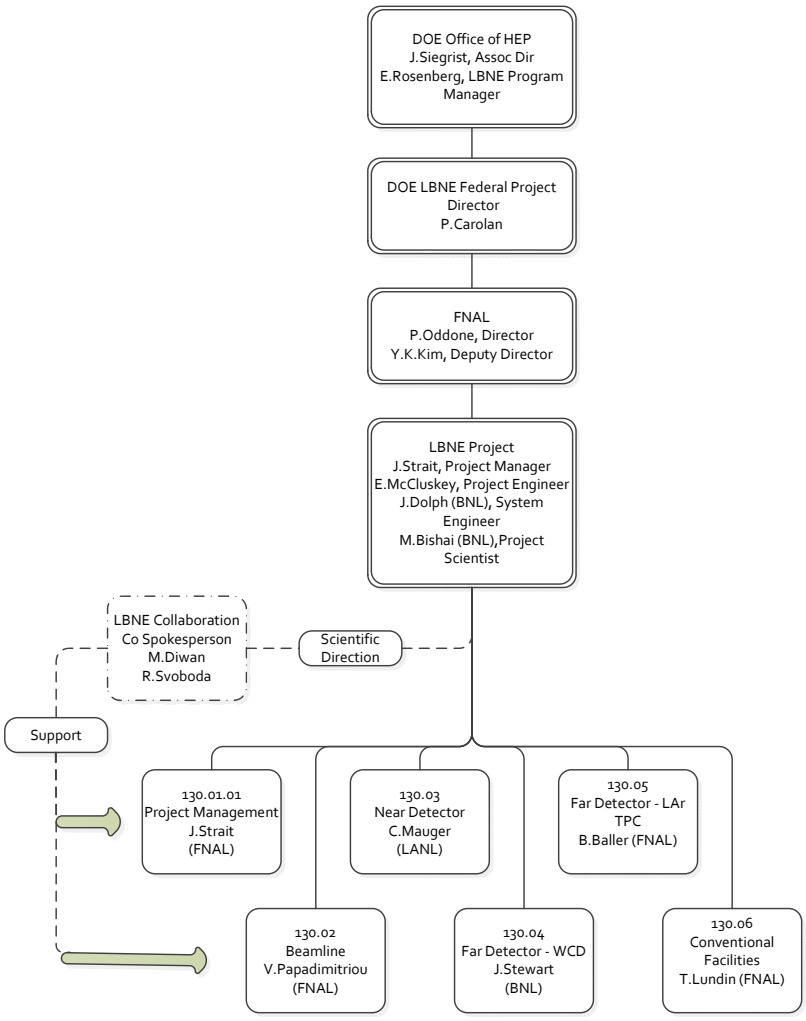

Figure 4–1: LBNE Project Organization Chart

4.2 Work Breakdown Structure

The LBNE Work Breakdown Structure (WBS) is a means of organizing the work scope of the Project. A WBS decomposes the Project's tasks and deliverables into smaller, manageable components. We define the overall LBNE Project ("Project 130" within the Fermilab-wide WBS) as WBS Level 1, and each of its subprojects, listed above, as Level 2. The subprojects, in turn, get broken out into lower, component levels. Table 4–1, shows the LBNE WBS down to Level 3 (it does not include the Water Cherenkov Far Detector).

Table 4–1: WBS Chart (WBS Element Numbers and Names) to Level 3

Number	Name
130	**LBNE**
130.01	**LBNE Project Office**
130.01.01	LBNE Conceptual Design
130.01.02	LBNE Preliminary Design
130.01.03	LBNE Final Design
130.01.04	LBNE Construction
130.01.05	LBNE Closeout
130.02	**Beamline**
130.02.01	Beamline – Project Management
130.02.02	Beamline – Primary Beam
130.02.03	Beamline – Neutrino Beam
130.02.04	Beamline – System Integration
130.03	**Near Detector Complex (NDC)**
130.03.01	NDC – Project Management
130.03.02	NDC – Measurement Strategy
130.03.03	NDC – Beamline Measurements
130.03.04	NDC – Neutrino Detectors
130.03.05	NDC – Detector Magnet
130.03.06	NDC – Global DAQ and Computing Systems
130.05	**Liquid Argon Far Detector (LAr)**
130.05.01	LAr – Project Management
130.05.02	LAr – Cryogenics and Cryostat
130.05.04	LAr – Time Projection Chamber
130.05.05	LAr – DAQ and Monitoring
130.05.06	LAr – Installation and Commissioning
130.05.07	LAr – Photon Detector
130.05.09	LAr – LAr1 1-kton Engineering Prototype
130.06	**Conventional Facilities (CF)**
130.06.01	CF – Project Management
130.06.02	CF – Near Site (Fermilab)

130.06.04	CF – Far Site (Sanford Lab)

4.3 Project Cost and Schedule

The initial cost range of the LBNE Project is $1,150M to 1,750M, with a target total project cost (TPC) for execution of $1,521M with contingency in base-year (FY10) dollars. The target execution schedule is 15 years from CD-0 to CD-4, beginning with CD-0 in January 2010, which includes one year of schedule contingency that has been backend-loaded.

Table 4–2: Target Budget Cost Estimates at WBS Level 2

WBS	Description	TPC (in $k)	TPC % Contingency
130.01	Project Management Office	72,796	30%
130.02	Beamline	180,247	36%
130.03	Near Detector Complex	43,548	29%
130.04	Water Cherenkov Far Detector	11,153	0%
130.05	LAr Far Detector	410,629	41%
130.06	Conventional Facilities	803,567	41%
Estimated Total Project Cost (TPC)		1,521,939	39%

5 Project Scope

5.1 Overview

The DOE Mission Need for the LBNE Project proposes the following major elements:

- an intense neutrino beam aimed at a far site
- detectors located at the near site just downstream of the neutrino source
- a massive neutrino detector located at the far site

The LBNE Project scope includes construction of experimental systems and facilities at two separate geographical locations. We present a reference design for achieving LBNE's mission in which a proton beam extracted from the Fermilab Main Injector (MI) is used to produce a neutrino beam. The neutrino beam traverses near detectors a few hundred meters downstream before traveling through the Earth's mantle to a detector located 1,300 km away in the Sanford Underground Laboratory, the site of the former Homestake Mine in Lead, South Dakota. The 1,300-km separation between the sites presents an optimal baseline for LBNE's neutrino-oscillation physics goals.

The main scope elements on the Fermilab site, also referred to as the Near Site, include:

- magnets and support equipment to transport the extracted protons to the target (where approximately 85% of them interact, producing pions and kaons)
- a target and target hall
- magnetic focusing horns to direct pions and kaons into a decay tunnel
- a decay pipe where these particles decay into neutrinos
- a beam absorber at the end of the decay pipe to absorb the residual secondary particles

- near detectors to make beamline measurements and neutrino-flux and spectrum measurements
- conventional facilities at Fermilab to support the technical components of the primary proton beam, the neutrino beam and the near detectors

The main scope elements at the Sanford Laboratory site, the Far Site, include:

- the massive Far Detector, located underground
- infrastructure required for the Far Detector, both above- and below-ground
- conventional facilities at Sanford Laboratory to house and support the technical components of the Far Detector

5.2 Beamline at the Near Site

The LBNE Beamline at Fermilab will be designed to provide a neutrino beam of sufficient intensity and energy to meet the goals of the LBNE experiment with respect to long-baseline neutrino-oscillation physics. The design is that of a conventional, horn-focused neutrino beamline. The components of the beamline will be designed to extract a proton beam from the Fermilab Main Injector and transport it to a target area where the collisions generate a beam of charged particles. This secondary beam, aimed toward the Far Detector, is followed by a decay pipe where the particles of the secondary beam decay to generate the neutrino beam. At the end of the decay pipe, an absorber pile stops the residual particles.

The facility is designed for initial operation at proton-beam power of 708 kW, with the capability to support an upgrade to 2.3 MW. In the reference design, extraction of the proton beam occurs at MI-10, a new installation. After extraction, this primary beam establishes a horizontally straight compass heading west-northwest toward the Far Detector, but will be bent upward to an apex before being bent downward at the appropriate angle, 101 milliradians (5.79°) as shown in Figure 5–1. The primary beam will be above grade for about 700 feet; this design minimizes expensive underground construction and significantly enhances capability for ground-water radiological protection.

The target marks the transition from the intense, narrowly directed proton beam to the more diffuse, secondary beam of particles that in turn decay to produce the neutrino beam. The interaction of a single proton in the target creates, on average, four charged particles consisting mostly of pions and kaons. These secondary particles are short-lived. Each secondary particle decay generates a muon, which penetrates deep into the surrounding rock and a neutrino that continues on toward the Near and Far Detectors.

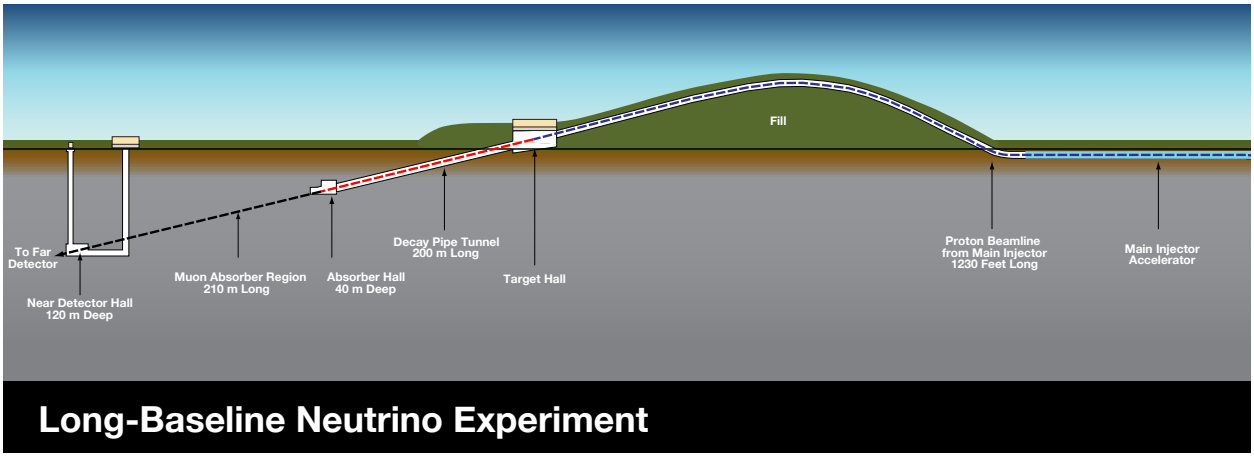

Figure 5–1: Schematic of the systems included in the LBNE Beamline subproject. The top of the engineered hill is 22 m above grade, somewhat less than half the height of Wilson Hall, shown on the right in the distance.

After collection and focusing, the pions and kaons that did not initially decay – the residual particles mentioned above – need a long, unobstructed volume in which to decay. This decay volume in the reference design is a pipe of circular cross section with its diameter and length optimized such that decays of the pions and kaons result in neutrinos in the energy range useful for the experiment.

5.3 Near Detector Complex

The LBNE Near Detectors, located downstream of the target, consist of two detector systems, one for making measurements of muons in the beamline and the other to measure the neutrino spectrum, interactions and kinematics. The Near Detectors' primary purpose is to maximize the oscillation physics potential of the Far Detector. The scope and design of the Near Detectors are therefore driven by the overall experiment's requirements for the neutrino-oscillation analysis, which will not yet be known precisely by CD-1. In general, however, the Near Detectors must: (1) measure the intrinsic ν_e component of the beam with sufficient precision to allow subtraction of this irreducible background, and (2) measure the detailed final-state kinematics of neutrino interactions of the LBNE beam on argon nuclear targets with sufficient precision to allow prediction of the particle identification efficiency in the Far Detector.

The Beamline Measurements system (BLM) will be placed in the region of the absorber at the downstream end of the decay region. Three detector systems will be deployed to measure (1) the muon-beam profile (with a grid of ion chambers), (2) the muon-beam energy spectrum (using variable-pressure threshold gas Cherenkov detectors), and (3) the muon flux (by counting the number of muon-decay Michel electrons in "stopped-muon" detectors).

These measurements constrain the beam neutrino flux and are used in conjunction with the Near Detector measurements to extract more detailed information on neutrino cross-sections and final-state interactions.

The Neutrino Measurements system will be placed underground in the Near Detector Hall 450 m downstream of the target. The reference design consists of a liquid argon time projection chamber tracker (LArTPCT), based on the MicroBooNE design. The detector apparatus will be enclosed in a wide-aperture dipole magnet based on the design of the CERN UA1 [10] magnet. The magnetic field will enable charge-sign determination of particles from their bend direction as they traverse the detector. Interspersed in the magnet yoke and surrounding the magnet will be a plastic-scintillator muon-identification system (MuID).

5.4 Conventional Facilities at the Near Site

The baseline design for the LBNE Project at the Near Site incorporates extraction of a proton beam from the MI-10 point of the Main Injector, which then determines the location of the NDC and supporting Near Site Conventional Facilities. The Near Site Conventional Facilities not only provide the support buildings for the underground facilities, but also provide the infrastructure to direct the beamline from the below-grade extraction point to the above-grade target. See Figure 5–1 for a schematic of the experimental and conventional Near Site facilities.

Figure 5–2 shows a schematic longitudinal section of the entire Near Site, with an exaggerated vertical scale of 3 to 1 to show the entire Project alignment in one illustration.

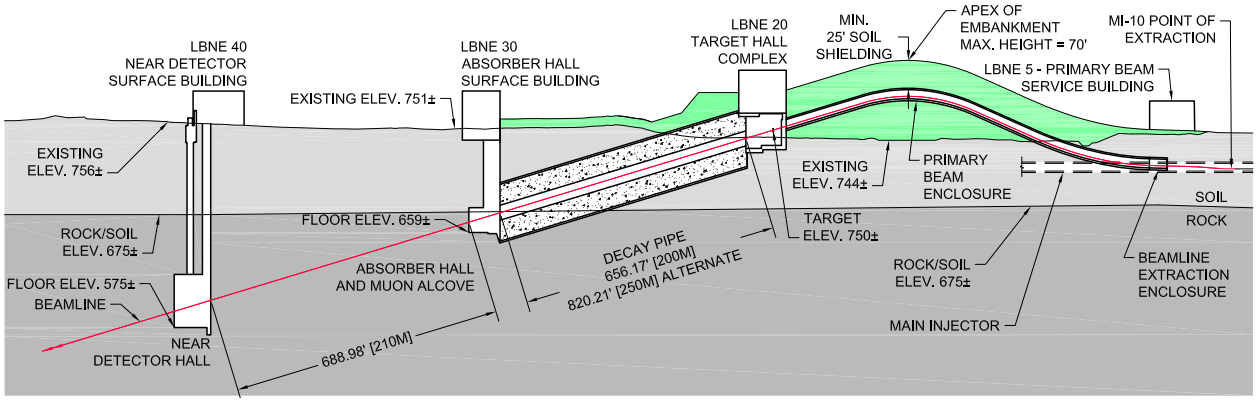

Figure 5–2: LBNE Near Site schematic longitudinal section view

The beam will travel approximately 1,200 ft (366 m) through the proposed Primary Beamline Enclosure to the Target Hall Complex and through focusing horns and a target to create an intense neutrino beam. This beam will traverse a 656-ft (200-m) long decay pipe followed by

a hadron absorber; at this point the beam leaves the Absorber Hall and travels 689 ft (210 m) through bedrock to range out (absorb) muons before reaching the Near Detector Hall. The neutrino beam will then pass through the Near Detectors before continuing through the Earth's mantle to the Far Site.

The Near Site Conventional Facilities LBNE Project layout at Fermilab, the "Near Site", is shown in Figure 5–3. Following the beam from east to west, or from right to left in this figure, is the underground Primary Beamline Extraction Enclosure, the underground Primary Beamline Enclosure/Pre-target Tunnel and its accompanying surface based Service Building (LBNE 5), the in-the-berm Target Hall Complex (LBNE 20), the Decay Pipe, the underground Absorber Hall and its surface Service Building (LBNE 30), and the underground Near Detector Hall and its surface Service Building (LBNE 40). The Project limits are bounded by Giese Road to the north, Kautz Road to the east, Main Injector Road to the south, and Kirk Road to the west.

Figure 5–3: LBNE overall project Layout at Fermilab

These facilities are described in detail in Volume 5 of this CDR.

5.5 Liquid Argon Far Detector

The LBNE Far Detector is being designed as a liquid argon time projection chamber (LArTPC). LArTPCs combine fine-grain tracking with total absorption calorimetry to enable precision neutrino-event detection in scalable neutrino detectors. The millimeter-scale spatial resolution combined with recordable dE/dx provides excellent signal efficiency and background rejection for both beam and non-beam neutrino physics.

The signal in liquid argon is generated by a well known electromagnetic process, the generation of ionization electrons by the passage of particles through liquid argon. The fraction of electrons that recombine and the trajectory of the electrons are determined by the electric field in the drift region.

The LBNE LArTPC, referred to as the LAr-FD, consists of two massive cryostats in a single cavern, oriented end-to-end along the beam direction (roughly east-to-west), and located at the 4850 level (4850L) of the Sanford Laboratory. Each cryostat is a rectangular vessel 24 m wide, 16.0 m high and 49.0 m long and they are separated by a 15-m clear space with thick septum walls. The fiducial mass of each, as defined for neutrino-oscillation studies, is 16.3 kton and the active (instrumented) mass is 20 kton, resulting in a total active mass of 40 kton. The detector's configuration is illustrated in Figure 5–4.

The detector includes a cryogenic system that keeps the liquid argon at a temperature of 89 K and maintains the required purity using a pump and filter system.

The detection system in each cryostat consists of a time projection chamber (TPC) and readout electronics. A TPC consists of rows of cathode planes interleaved with rows of anode planes between sets of which uniform electric fields are created. See Figure 5–5. Charged particles passing through the TPC release ionization electrons that drift along the field to the anode planes. The bias voltage is set on the anode wires (of which there are four layers) such that ionization electrons drift between the first several layers (called *induction* layers) and are collected on the last layer (the *collection* layer).

Readout electronics amplify and continuously digitize the induced waveforms on the sensing wires at several MHz, and transmit these data to the data acquisition (DAQ) system. The wire layers are oriented at different angles relative to each other allowing a 3D reconstruction of the particle trajectories.

5.6 Far Detector Depth

In 2008, the LBNE Science Collaboration undertook a detailed study of the depth requirements for the main physics topics of interest with large detectors. This work is referred to

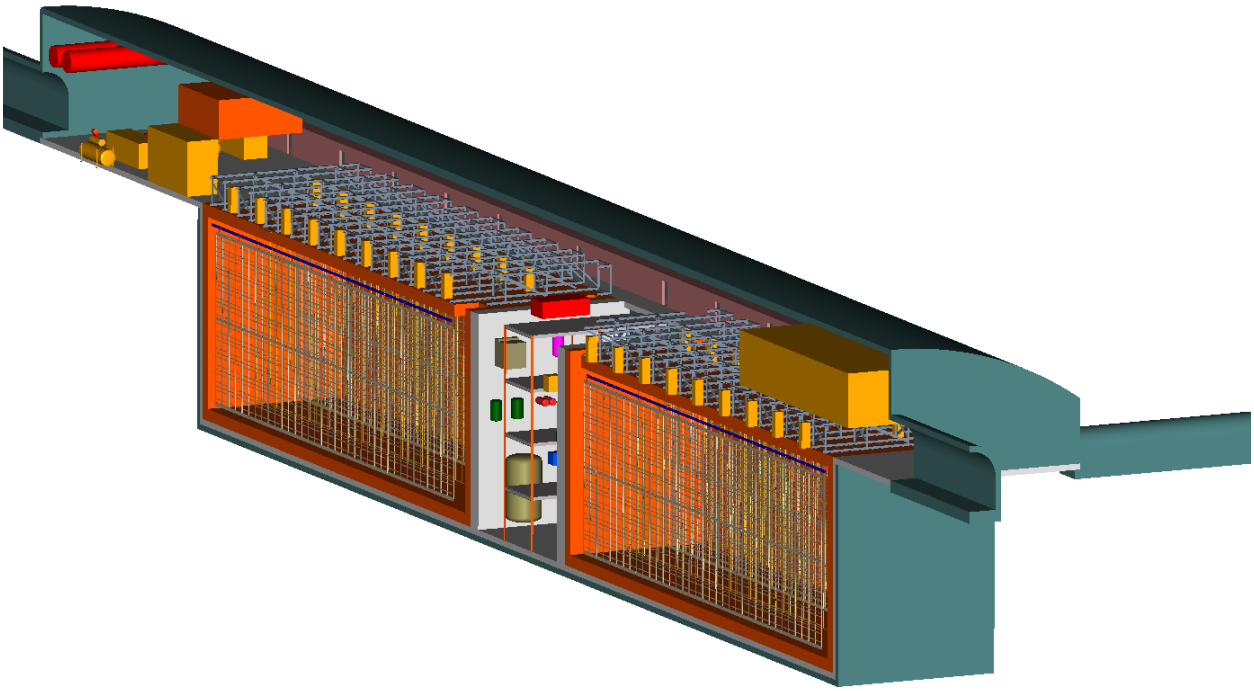

Figure 5–4: LAr-FD configuration within cavity

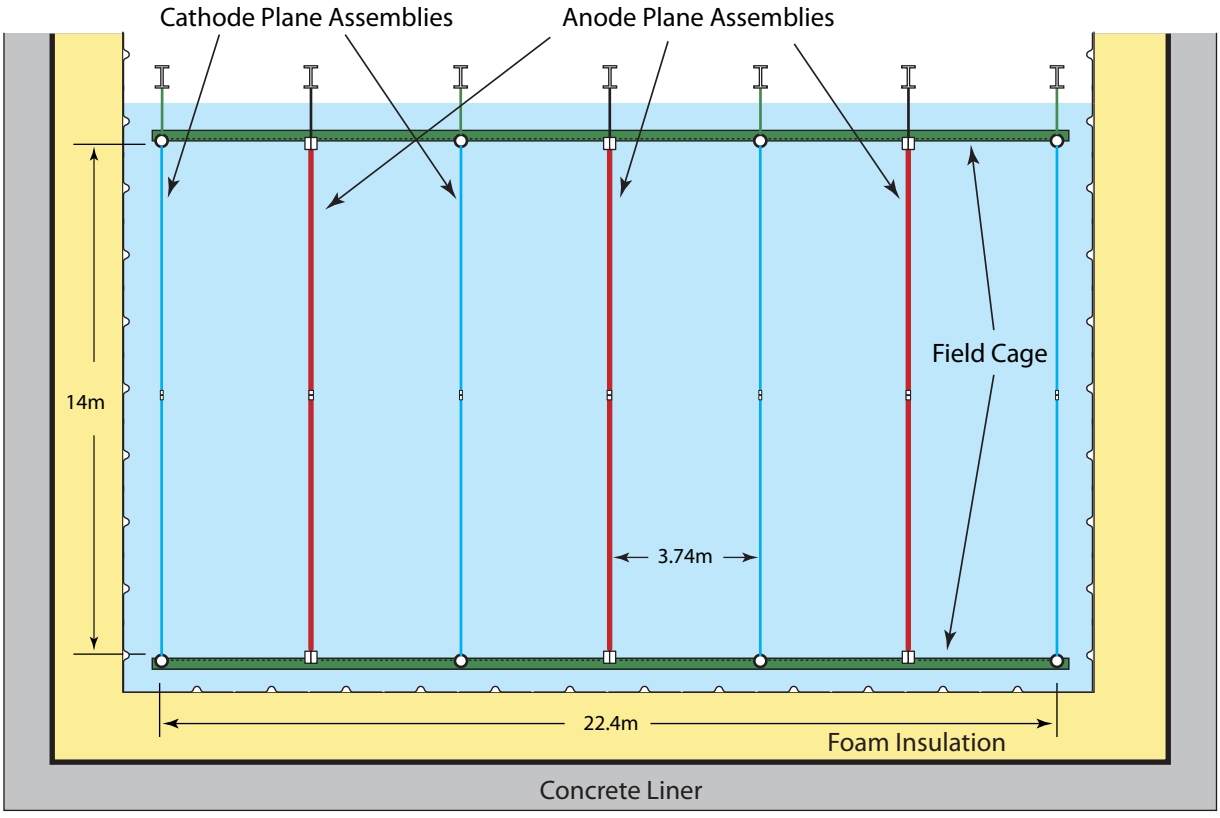

Figure 5–5: TPC cross section view

as "The Depth Document" [11]. The topics considered were accelerator-generated neutrinos; supernova, solar and atmospheric neutrinos; and nucleon decay. The requirement on the depth of the detector is guided by the rate of the desired signals and the rate of backgrounds from cosmic rays over a very wide range of energies (from solar-neutrino energies of 5 MeV to high energies in the hundreds of GeV.)

Table 5–1 lists the depth requirements for this detector to accomplish LBNE's goals for each physics measurement.

Table 5–1: Depth requirement (in meters-water-equivalent) by physics topic for a Liquid Argon TPC

Physics Topic	Depth (mwe)
Long-baseline accelerator	0 – 1,000
$p \to K^+\nu$	$>$ 3,000
Day/Night ^{8}B Solar ν	$\sim$ 4,300
Supernova burst	3,500
Relic supernova ν	$>$ 2,500
Atmospheric ν	2,400

5.7 Conventional Facilities at the Far Site

The Far Site used in our reference design is the Sanford Underground Laboratory at Homestake, in Lead, S.D.

The scope of the underground facilities required for the LAr includes new excavated spaces at the 4850L for the detector, utility spaces for experimental equipment, utility spaces for facility equipment, drifts for access, Area of Refuge (AoR) for emergencies, as well as construction-required spaces. Underground infrastructure for the facility includes power to experimental equipment, domestic water, industrial water for process and fire suppression, ventilation and exhaust, fire detection and alarm, normal and standby power systems, sump pump drainage system for conveying native infiltration water to the facility-wide pump discharge system, and cyberinfrastructure for communications and security. In addition, existing infrastructure that must be upgraded to meet LBNE needs include rehabilitation of the Ross and Yates Shafts from the surface down to the 4850L. Rehabilitation of the Ross Shaft is scheduled to begin in 2012, well ahead of any LBNE-related construction. In addition, the Oro Hondo Shaft must be extended from 3650 to the 4850L, as depicted in Figure 5–6.

The detector requires a cavity excavation of a rectangular shape with dimensions of 27 m $\times$ 18 m $\times$ 121 m. Just above the detector, a domed excavated space of 33 m $\times$ 14 m $\times$ 161 m is required for a service area, as shown in Figure 5–6.

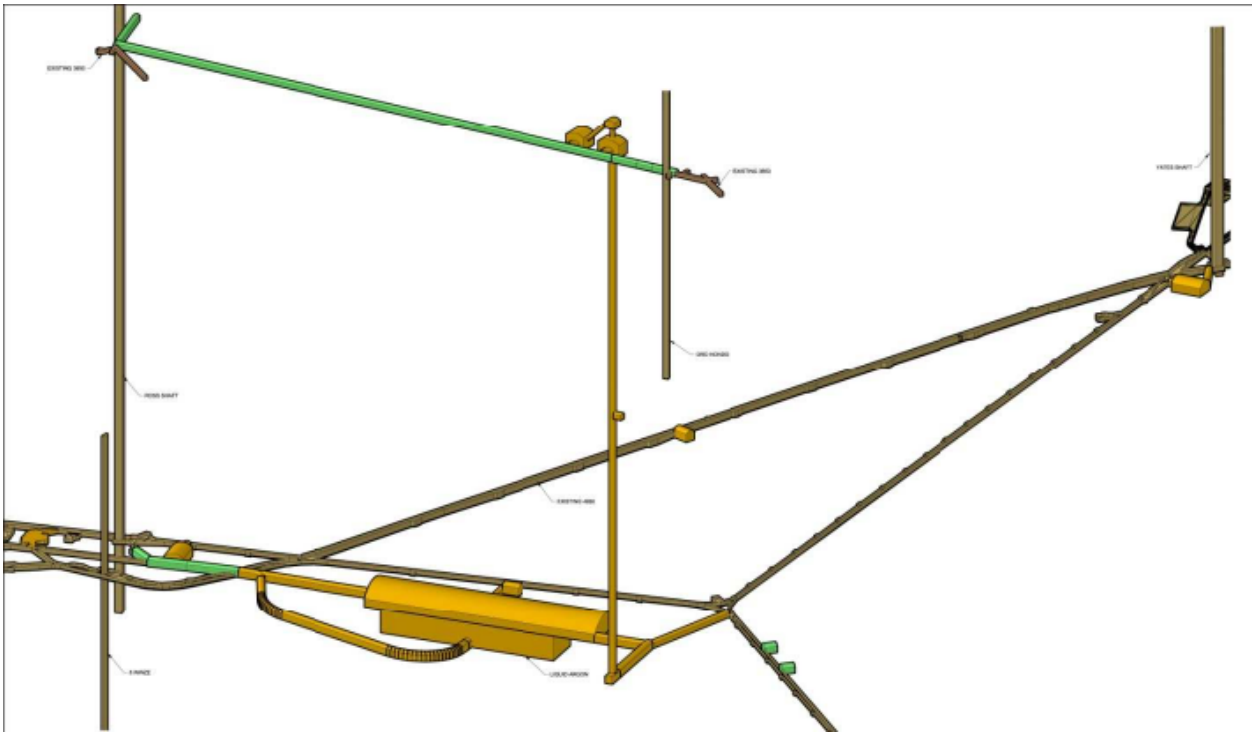

Figure 5–6: Schematic of underground conventional facilities for an LArTPC at the 4850L

The existing Sanford Laboratory has many surface buildings and utilities, some of which can be utilized for LBNE. The scope of the above ground work for Conventional Facilities includes only that minimal work necessary for LBNE, and not for the general rehabilitation of buildings on the site, which remains the responsibility of the Sanford Laboratory.

6 Experimental Capabilities

6.1 Overview

The primary science objectives for LBNE as described in Chapter 3 dictate the need for very large mass, 100 kiloton-scale neutrino detectors located at large depth at a distance of $>$ 1000 km from the neutrino source at Fermilab. A large mass is required to accumulate enough neutrino interactions – $\mathcal{O}(1000)$ events – for precision measurements of the parameters that govern $\nu_\mu \rightarrow \nu_e$ oscillations as well as for providing sufficient nucleons to enable the search for proton decay.

The significant depth [11] is necessary to reduce backgrounds to a sufficient level for low-energy physics searches such as proton decay and supernova neutrinos. To meet both the primary and secondary physics objectives, the detector is required to have excellent particle identification over a wide range of particle energies from a few GeV (for measuring long-baseline beam neutrino oscillations and atmospheric neutrinos) to a few MeV (for identification of supernova, solar and geophysical neutrinos).

Neutrino events detected in experiments like LBNE are often categorized according the particle mediating the interaction. The term (used below, and throughout this document) "neutral current process" (NC) refers to an interaction which is mediated by the neutral boson Z^0. Similarly, a "charged current" (CC) interaction involves a postive or negative charged W boson. The flavor of a neutrino in a CC interaction is tagged by the flavor of the emitted lepton: e, μ, τ tag ν_e, ν_μ, ν_τ interactions. CC and NC interactions of neutrinos with energies > 1 GeV are inelastic and the target nucleus disintegrates producing multiple hadrons.

A substantial component of the background for ν_e CC interactions comes from NC interactions where a π^0 is produced. The π^0 decays to two γs which shower electromagnetically and fake electrons. NC interaction interactions where a charged pion is produced are also the predominant background for ν_μ CC interactions where the pion fakes a muon. Therefore to study neutrino flavor oscillations with high precision, the LBNE Far Detector has to have high efficiency, high purity $e/\mu/\gamma$ and $\pi/K/p$ separation.

A "quasi-elastic" (QE) event is a CC event in which the scattering of the neutrino is almost elastic with only a charged lepton and a nucleon or nucleons emerging from the target nucleus. The charged lepton in QE events carries most of the energy of the neutrino, and as a result, QE interactions have the best neutrino-energy resolution. Final State Interactions (FSI) inside the nucleus will alter the expected nucleon types and spectrum, and measurement of this effect is an important goal of the Near Detector.

A massive liquid argon TPC (LArTPC) has been chosen as the Far Detector technology for the LBNE project. TPCs are the detectors of choice for low-rate, large-volume, high-precision particle physics experiments due to their excellent 3D position resolutions and particle identification in large volumes. In addition to detailed event topologies and measurements of particle kinematics, dE/dx measurements allow TPCs to unambiguously distinguish electrons, muons, photons, kaons, pions and protons (see Figure 6–1) over a wide range of energies.

A massive LArTPC with a fiducial volume of 34 kton as the LBNE Far Detector fulfills the high-mass requirement coupled with the excellent particle identification over a wide range of energies expected from a large volume TPC. The photo-detection system will detect scintillation light in order to: (1) determine the exact time of the start of the drift process, and (2) provide a trigger for the proton decay, supernova, and other non-beam physics.

The large mass and the location of the LBNE Liquid Argon TPC at the 4850L of the Sanford Laboratory enables searches for processes beyond the Standard Model predicted by several grand unified theories (GUTs). In particular, the identification of kaons with high purity in a TPC enables measurements of proton decays with a charged kaon in the final state.

The high mass and timing resolution of the detector enable detailed energy and time-dependent measurements of supernova-burst neutrinos, should one occur within our galaxy. Atmospheric and beam neutrinos share the same requirements for particle identification, but atmospheric neutrinos provide an independent sample of neutrinos oscillating over much longer distances. Solar neutrinos require very low thresholds (< 10 MeV) which could be achieved if radioactive contaminants in the TPC can be minimized.

The LBNE project includes Near Detectors located just downstream of the neutrino source. Their primary purpose is to measure the un-oscillated rate of beam neutrinos with high precision. The combination of high-precision neutrino-beamline measurements (using a high-resolution near neutrino detector) and a high-intensity, on-axis, wide-band neutrino beam will also enable LBNE to carry out a rich program of short-baseline neutrino physics and outperform current short baseline experiments.

In this chapter, we present a summary of the experimental capabilities and performance metrics of LBNE. The "Fall 2010 Report from the Physics Working Group" [6] has a detailed study of the extensive physics capabilities of LBNE. The LBNE Case Study Report for a Liquid Argon TPC [9] has further details on the performance metrics of the LAr-TPC.

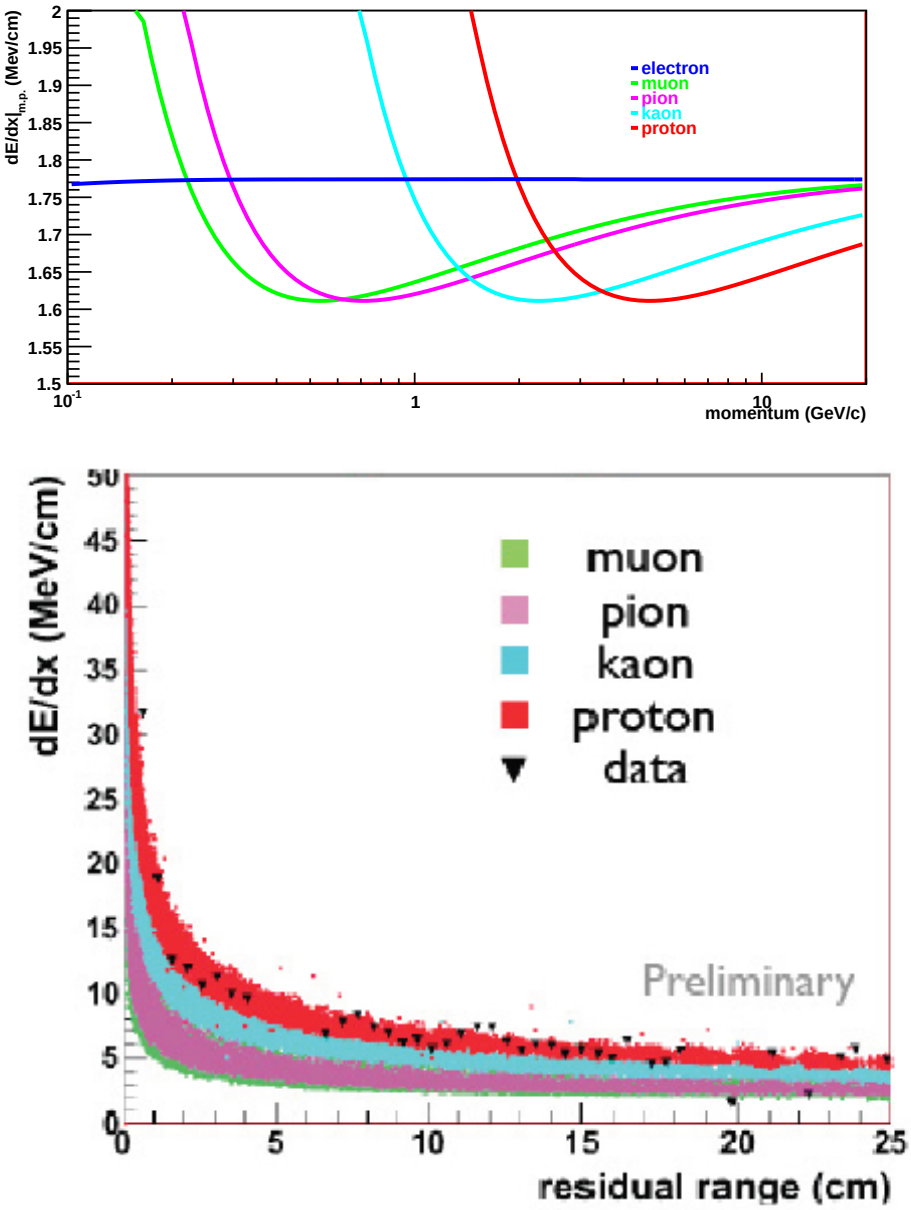

Figure 6–1: Distributions of dE/dX values for different charged particle species from a GEANT4 simulation of a liquid Argon TPC. The top plot is the most probable value of dE/dX vs particle momentum. The bottom plot is the value of dE/dX versus residual range from a GEANT4 simulation. The points are proton dE/dX measurements obtained from ArgoNEUT.

6.2 Accelerator-based Long-Baseline Neutrino Oscillations

The primary scientific objective for LBNE is the precision measurement of the parameters that govern neutrino oscillations over a long baseline exceeding 1000 km. The observation and measurement of the characteristics of $\nu_\mu/\bar{\nu}_\mu \rightarrow \nu_e/\bar{\nu}_e$ oscillations in the neutrino-energy region from 0.5 to 5 GeV at 1,300 km would enable the unambiguous determination of the neutrino mass hierarchy and the measurement of δ_{cp}, the CP phase. The $\nu_\mu \rightarrow \nu_e$ oscillation probability (colored curves) at 1,300 km for $\sin^2 2\theta_{13} = 0.1$ and various values of the CP violating phase δ_{cp} are shown in Figure 6–2. The shaded histogram is the unoscillated ν_μ CC spectrum at 1,300 km obtained from the LBNE conceptual beam design where the first focusing horn design has been further optimized to maximize the rate of ν_es appearing at the Far Detector. This beam design assumes a 250-m decay length (the reference design value has since been set at 200 m, but increasing it is under consideration).

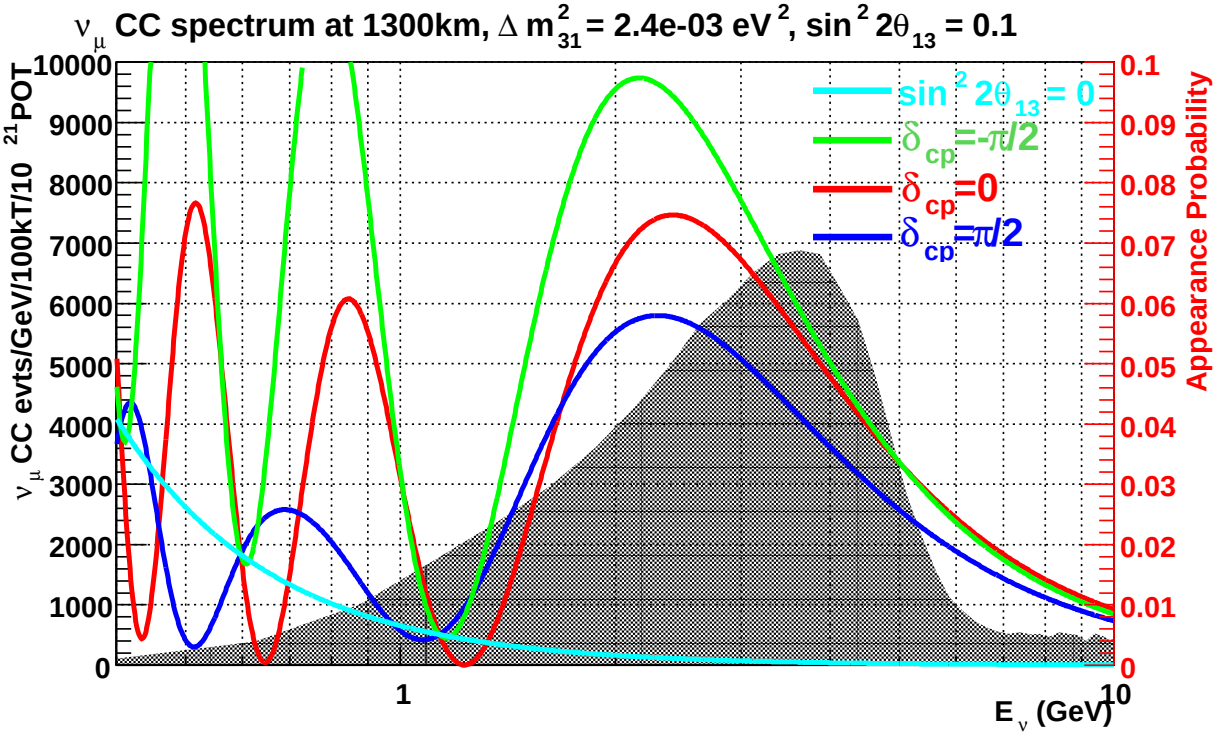

Figure 6–2: The $\nu_\mu \rightarrow \nu_e$ oscillation probability (colored curves) at 1300km for $\sin^2 2\theta_{13} = 0.1$ and various values of the CP violating phase δ_{cp}. The shaded histogram is the unoscillated ν_μ CC spectrum at 1300km from the low-energy (LE) beam tune. This beam tune includes a 250m decay pipe and further optimization of LBNE horn 1 and target designs.

In Table 6–1, the neutrino-interaction rates for all three known species of neutrinos as expected at the LBNE Far Detector site are listed. We have assumed a tunable beam spectrum obtained by changing the distance between the target and the optimized horn 1 design.

Target Position	ν_μ CC	ν_μ CC osc	ν_μ NC	ν_e CC beam	$\nu_\mu \rightarrow \nu_e$ CC	$\nu_\mu \rightarrow \nu_\tau$ CC
-0.3 m (LE tune)	29K	11K	4.1K	260	1300	140
-1.5 m (ME tune)	44K	28K	8.4K	320	1100	640
-2.5 m (HE tune)	47K	35L	9.6K	280	770	800

Table 6–1: ν_μ, ν_τ, ν_e interaction rates per 100 kton.MW.yr (10^{21} protons-on-target) at the Far Detector site in LBNE for different beam tunes obtained by moving the target w.r.t. horn 1. Normal hierarchy, $\sin^2 2\theta_{13} = 0.1$. The rates are integrated in the region 0.5-20 GeV. The first column of numbers is the unoscillated ν_μ total charge-current interaction rate. The second column of numbers is the rate of ν_μ CC interactions expected given $\nu_\mu \rightarrow \nu_\mu$ oscillations.

6.2.1 Measurements of Mass hierarchy and the CP Violating Phase

A primary science objective of LBNE is to make precise measurments of the parameters that govern $\nu_\mu \rightarrow \nu_e$ oscillations. These parameters probe CP violation in the neutrino sector and determine the neutrino mass hierarchy. The sensitivity of the LAr-FD for ν_e appearance physics is primarily dependent on the signal efficiency for detecting electron-neutrino interactions and the background rejection of neutral current (NC) events and ν_μ charged current (CC) events in the range of 500 MeV to 5 GeV. NC events containing π^0s are the dominant source of background from NC interactions. The π^0 decays to two photons which convert to e^+e^- pairs and initiate an electromagnetic shower that can be difficult to distinguish from an electron shower. High-efficiency and high-purity with e/γ separation is required to distinguish ν_e CC from ν NC events. Excellent μ/e separation is also required to enable the distinction of ν_μ and ν_e CC interactions. In addition to measurements of the CP parameters, LBNE will search for physics beyond the Standard Model with high-precision measurements of the parameters Δm^2_{32} and $\sin^2 2\theta_{23}$ in ν_μ and $\bar{\nu}_\mu$ long-baseline oscillations. These measurements require high-purity identification of ν_μ CC interactions for which high-precision separation of $\mu/\pi/p^+$ is necessary. The strength of the LAr-FD is the ability to use detailed event topology, particle kinematics, and dE/dX to differentiate ν_e, ν_μ CC and NC π^0 event classes with high purity and efficiency as illustrated in Figure 6–3.

The expected performance of the LAr-FD is extrapolated from the analysis results obtained from four independent studies of massive LArTPCs. The four studies are detailed in references [13] [14] [15] [16] and are summarized in Table 6–3.

The most detailed LArTPC performance parameters to date were obtained from studies by the ICARUS collaboration [17] and the 2-km detector proposal for the T2K experiment [13]. The simulated geometry of the TPC for the 2-km T2K proposal is summarized in Table 6–3. This study is the only one to use fully automated 3D event reconstruction combined with dE/dx particle id and event kinematics in an automated analysis. The neutrino-event reconstruction and analysis were optimized to separate ν_μ CC and ν_μ NC separation, but did not include e/π^0 separation. As a result, the observed rate of 6.9% of NC events misidentified as ν_e CC is an over-estimate. A separate likelihood analysis of single electrons and π^0 interac-

Table 6–2: Estimated range of the LAr-TPC detector performance parameters for the primary oscillation physics. Signal efficiencies, background levels, and resolutions are obtained from the studies described in this chapter (middle column) and the value chosen for the baseline LBNE neutrino-oscillation sensitivity calculations (right column). * For atmospheric neutrinos this is the mis-identification rate for < 2 GeV events, the mis-identification rate is taken to be 0 for > 2 GeV.

Parameter	**Range of Values**	**Value Used for LBNE Sensitivities**
For ν_e CC appearance studies		
ν_e CC efficiency	70-95%	80%
ν_μ NC mis-identification rate	0.4-2.0%	1%
ν_μ CC mis-identification rate	0.5-2.0%	1%
Other background	0%	0%
Signal normalization error	1-5%	1%
Background normalization error	2-10%	5%
For ν_μ CC disappearance studies		
ν_μ CC efficiency	80-95%	85%
ν_μ NC mis-identification rate	0.5-10%	0.5%
Other background	0%	0%
Signal normalization error	1-5%	5%
Background normalization error	2-10%	10%
For ν NC disappearance studies		
ν NC efficiency	70-95%	90%
ν_μ CC mis-identification rate	2-10%	10% *
ν_e CC mis-identification rate	1-10%	10% *
Other background	0%	0%
Signal normalization error	1-5%	
Background normalization error	2-10%	
Neutrino energy resolutions		
ν_e CC energy resolution	$15\%/\sqrt{E(GeV)}$	$15\%/\sqrt{E(GeV)}$
ν_μ CC energy resolution	$20\%/\sqrt{E(GeV)}$	$20\%/\sqrt{E(GeV)}$
E_{ν_e} scale uncertainty		
E_{ν_μ} scale uncertainty	1-5%	2%

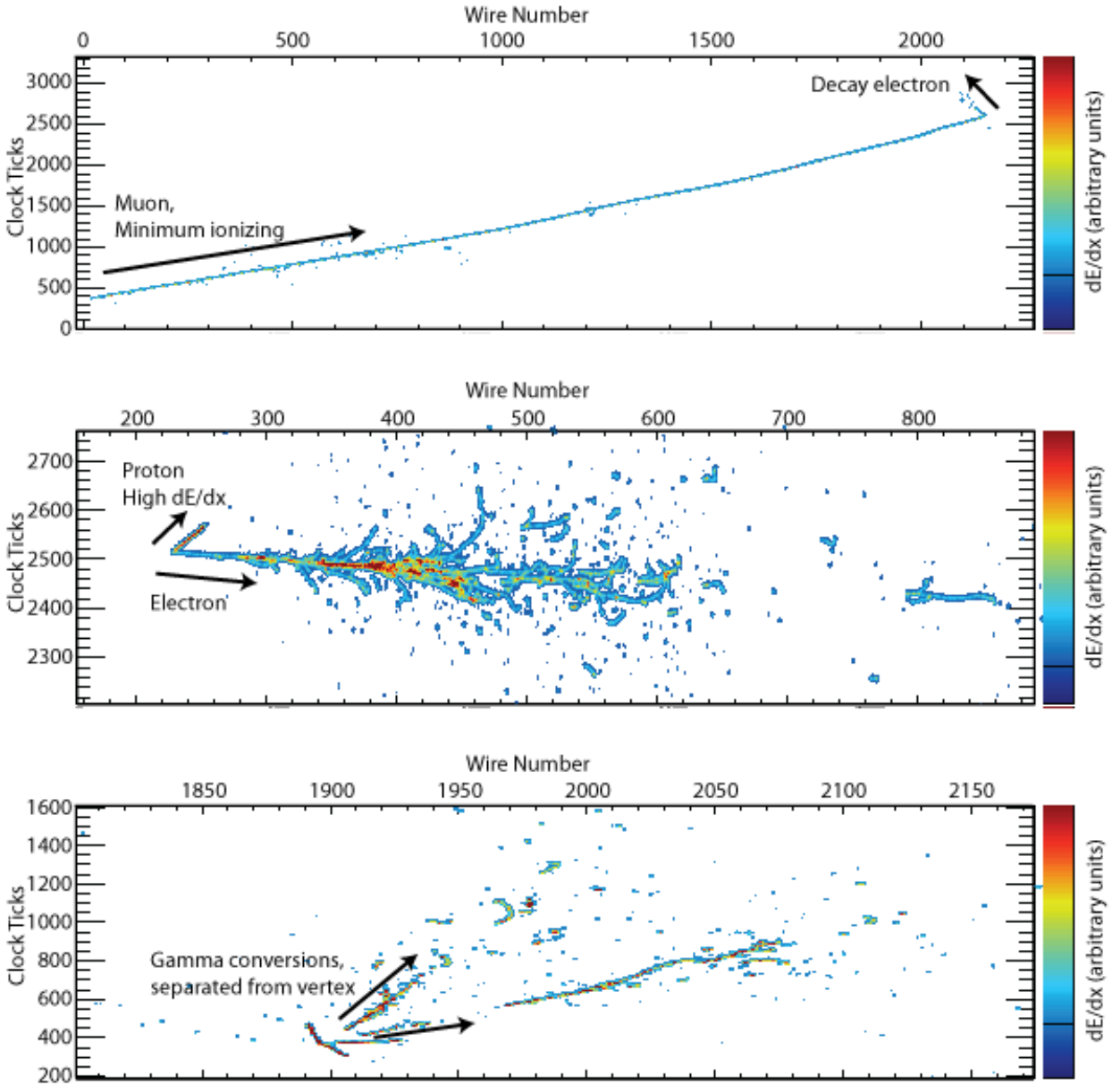

Figure 6–3: Examples of neutrino beam interactions in an LArTPC obtained from a GEANT4 simulation [12]. A CC ν_μ interaction with a stopped μ followed by a decay Michel electron (top), a QE ν_e interaction with a single electron and a proton (middle), an NC interaction which produced a π^0 that then decayed into two γ's with separate conversion vertices (bottom)

tions in the T2K 2-km LArTPC demonstrated that the single π^0 misidentification rate can be reduced to a few % using dE/dx alone as shown in Figure 6–4. Therefore, the 6.9% NC misidentification rate could be greatly reduced by including e/π^0 separation in the analysis.

The last three studies in Table 6–3 comprise visual scans of simulated events in which

Table 6–3: Description of the LAr-TPC simulations used to determine the performance for beam neutrino interactions.

Study	TPC geometry	Analysis technique
T2K 2km proposal [13] (2005)	140 tons, 4.5m(w)x4.5m(h)x5m(l) 2 readout chambers, 2 planes/chamber 3mm/6.4m wire pitch/length 2.21m/1.1ms max drift distance/time	Fully automated reconstruction, event topology, $\mu/\pi^{\pm}/K/p^{+}$ dE/dX and event kinematics included in a Random Forest analysis
Tufts Visual Scan [14] (2006)	Unknown	Blind visual scan visible energy precuts topology only
FNAL Visual Scan [15] (2008)	2.5m(w)x2.5m(h)x2.5m(l) 1 readout chamber, 2 planes/chamber 5mm and 10mm wire pitch	Blind visual scan MC truth used in precuts topology and dE/dX included in a log-likelihood analysis
FNAL Visual Scan [16] (2011)	MicroBooNE TPC	Blind visual scan topology only

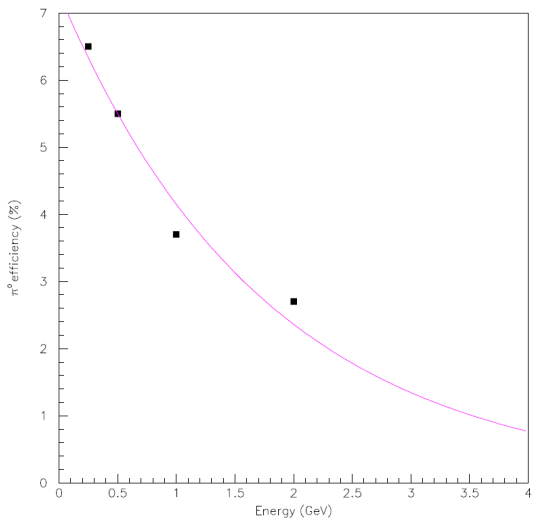

Figure 6–4: The electron mis-identification rate of single π^0 interactions as a function of the incoming π^0 energy [13].

researchers are trained to identify ν_e, ν_μ and NC π^0 interactions by studying event displays on an event-by-event basis. After training, the scanners are presented with a mixed sample of simulated events and asked to categorize them. Efficiencies are determined by comparing the scanners' results to the known event type. The selection efficiencies for signal neutrino interactions and rejection efficiencies for NC background, determined by the four studies summarized here, are shown in Table 6–4. There is a general agreement between all four

Table 6–4: Selection efficiencies for ν_e CC candidates and ν_e misidentification rates for ν_μ CC and ν_μ NC determined by various studies. The / symbol indicates samples where the event size was too small to draw meaningful conclusions.

Study	**Average** ν energy	**# events** studied	ν_e **CC** $\epsilon_{\rm select}$	ν_μ **CC** $\epsilon_{\rm mis-id}$	ν_μ **NC** $\epsilon_{\rm mis-id}$
T2K 2km proposal (2005)	0.25-4.0 GeV	2000	94.5%	2%	6.9%
Tufts Visual Scan (2006)	NOνA beam 1.5-4.5 GeV	450	$72 \pm 5\%$	/	$1.3 \pm 0.4\%$
FNAL Visual Scan (2008)	NOνA beam 0.5-3.5 GeV	4997	$92 \pm 9\%$	/	$0.6 \pm 0.1\%$
FNAL Visual Scan (2011)	Uniform 0.5-15 GeV	1501	$90 \pm 1\%$	$2.0 \pm 0.6\%$	$5 \pm 1\%$

studies that the efficiency for identifying ν_e CC events in the few-GeV range is in between 70 and 95%. In addition, function of neutrino energies has been found to be approximately flat for neutrino energies > 1 GeV, as shown in Figure 6–5. The misidentification rate of ν_μ CC events obtained from these studies is around 2%. Since optimized e/μ separation using dE/dx has not yet been implemented in these studies, the 2% ν_μ misidentification rate will be considered an upper limit.

There is a large variation observed in the NC misidentification rate. The lowest rate was obtained by the visual scan study that included a crude dE/dx measurement combined with topology [15]. The estimation of the NC misidentification rate is further complicated by the fact that only the last study in Table 6–4 simulated ν NC interactions with energies > 5 GeV. In the search for ν_e appearance by the MINOS experiment [18] – which has a beam-neutrino spectrum and ν_e signal range very similar to LBNE's – it was observed that $\approx 50\%$ of the NC background in the 1–5 GeV signal region originated from NC inelastic interactions with neutrino energies > 5 GeV. An example of the complicated topology of deep inelastic NC interactions is shown in Figure 6–6. Reliable estimates of the NC misidentification rate of such events are not available. Given the current knowledge of LArTPC performance from these studies, we estimate that the LBNE NC misidentification is between 2% (conservative) to 0.4% (aggressive) depending on how well e/π^0 separation techniques will perform in more complicated topologies.

For the neutrino-oscillation sensitivity calculations, information from these hand scans is used to set the detector-signal efficiencies and background-rejection efficiencies. Table 6–2 shows the range of ν_e selection efficiencies, background levels and neutrino energy resolutions from the hand scans in Table 6–4, along with the specific values chosen for the long-baseline oscillation-sensitivity projections.

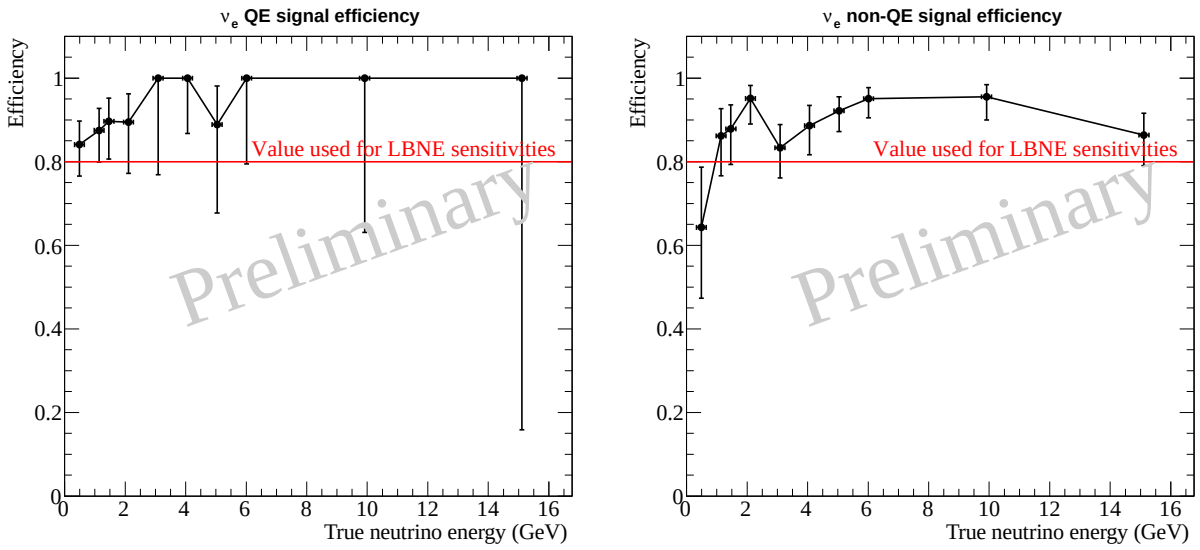

Figure 6–5: The efficiency, as determined by the 2011 Fermilab hand scan study [16] , of selecting ν_e CC quasi-elastic (left) and non-quasi-elastic(right) events.

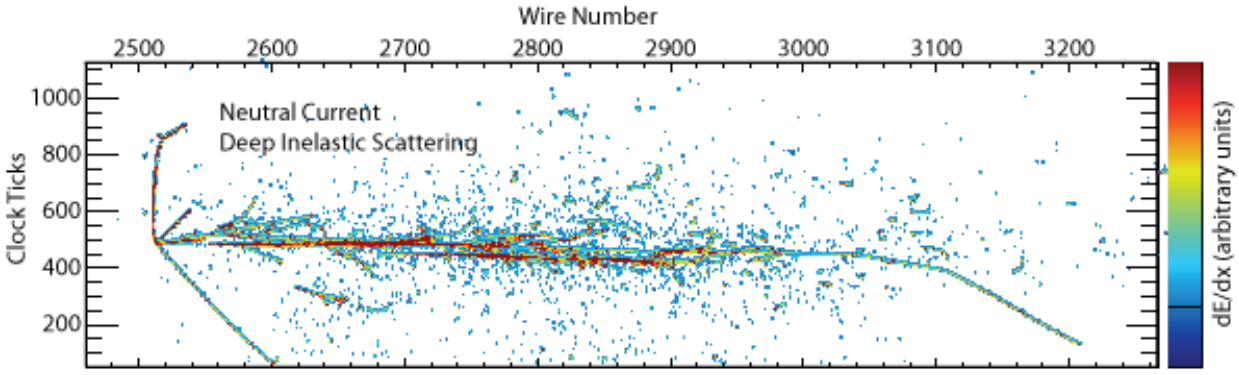

Figure 6–6: An example of a deep inelastic NC interaction in a LAr-TPC.

Studies from ICARUS have estimated and measured single-particle energy resolutions in LAr. Below 50 MeV, the energy resolution of electrons is $11\%/\sqrt{E[MeV]} + 2\%$. As shown in Figure 6–7, the energy resolution of an electromagnetic shower with energy in the range (50–5000) MeV is $33\%/\sqrt{E(MeV)} + 1\%$ [1]. The energy resolution of hadronic showers in an LArTPC is $\approx 30\%/\sqrt{E(GeV)}$. A significant fraction of the ν_e CC signal in LBNE in the range of 1–6 GeV is non-quasi-elastic CC interactions with a large component of the visible energy in the hadronic system. From recent simulations of neutrino interactions in the region of 1–6 GeV we have determined that the $< E_{\rm lepton}/E_\nu > \approx 0.6$. For this reason, the total electron-neutrino energy resolution for the neutrino-oscillation sensitivity calculation is chosen to be $15\%/\sqrt{E(GeV)}$. In a non-magnetized LArTPC the muon momentum can be

obtained from range and multiple scattering. The muon momentum resolution is found to be in the range $10 - 15\%$ [13] [19] for muons in the 0.5–3 GeV range. Therefore the total muon-neutrino energy resolution in LBNE is assumed to be $20\%/\sqrt{E(GeV)}$.

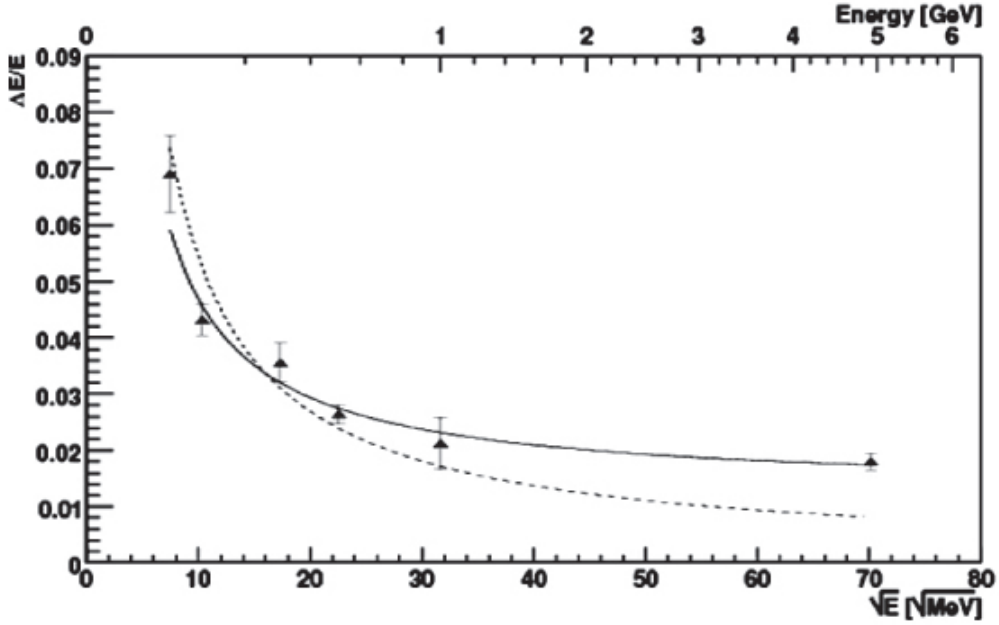

Figure 6–7: Resolution of electromagnetic showers from ICARUS [1]

In five years of neutrino (antineutrino) running, assuming $\sin^2(2\theta_{13}) = 0.1$, $\delta_{CP} = 0$, and normal mass hierarchy, we expect 1074 (229) selected $\nu_e(\overline{\nu}_e)$ signal events in the LAr-FD with a 708 kW beam. Table 6–5 is a summary of the expected number of signal and background events for ν_e and $\overline{\nu}_e$ running for normal and inverted hierarchy. The spectrum of expected signal and background events is shown in Figure 6–8.

Figure 6–9 shows the fraction of δ_{cp} values for which a 3σ resolution of the mass ordering (hierarchy) and determination of whether CP is violated ($\delta_{cp} \neq 0$ or π) is achieved by a 34-kton fiducial-volume LArTPC. For values of $\sin^2 2\theta_{13} > 0.07$, we find that LBNE will determine the mass hierarchy at the 5σ level. For values of $\sin^2 2\theta_{13} > 0.07$ LBNE will determine whether CP is violated for 65% and 40% of all δ_{cp} values at the 3 and 5σ levels respectively. The precision on the measurements of $\sin^2 2\theta_{13}$ and δ_{cp} that can be achieved is shown in Figure 6–10. LBNE will be able to measure δ_{cp} with a precision of better than 20° and $\sin^2 2\theta_{13}$ to better than 0.5%.

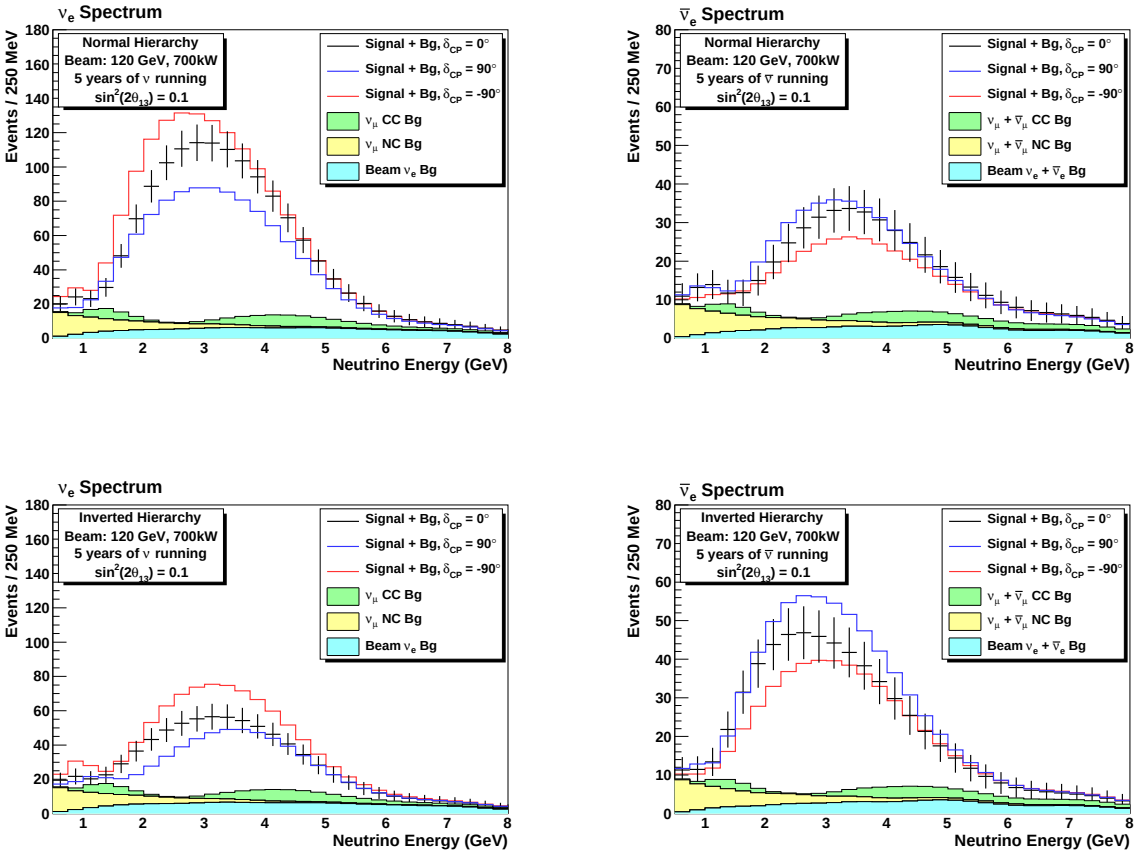

Figure 6–8: The expected spectrum of ν_e or $\overline{\nu}_e$ oscillation events in a 34-kton LArTPC for 5 years of neutrino (left) and antineutrino (right) running with a 700 kW beam, assuming $sin^2(2\theta_{13}) = 0.1$ for normal hierarchy (top) and inverted hierarchy (bottom). Backgrounds are displayed as stacked histograms.

6.2.2 Precision Measurements of the Oscillation Parameters in $\nu_\mu \rightarrow \nu_x$ Oscillations.

In addition to measurements of ν_e appearance, LBNE will make precise measurements of θ_{23} and $|\Delta m^2_{32}|$ using the $\nu_\mu/\bar{\nu}_\nu$-disappearance channel. Differences in the measured values of $|\Delta m^2_{32}|$ and $|\Delta \bar{m}^2_{32}|$ are sensitive to new physics arising from NC-like non-standard interactions [20] as described in Section 6.2.5.

The expected range of detector performance parameters for the ν_μ-disappearance channel are summarized in Table 6–2. The predicted spectrum of oscillated ν_μ and $\bar{\nu}_\mu$ CC events in LBNE is shown in Figure 6–11.

In Figure 6–12, the result from fits of the expected spectrum of $\nu_\mu/\bar{\nu}_\mu$ CC in the LBNE LAr-

Table 6–5: Expected number of neutrino oscillation signal and background events in the energy range (0.5 - 5.0) GeV at the LAr-FD, assuming $sin^2(2\theta_{13}) = 0.1$ and $\delta_{CP} = 0$.

	Signal Events	**Background Events**			
	ν_e	ν_μ CC	ν_μ NC	ν_e Beam	Total
Neutrino Normal Hierarchy	1074	66	77	92	234
Neutrino Inverted Hierarchy	477	66	77	97	240
Antineutrino Normal Hierarchy	279	29	51	46	126
Antineutrino Inverted Hierarchy	440	29	51	44	124

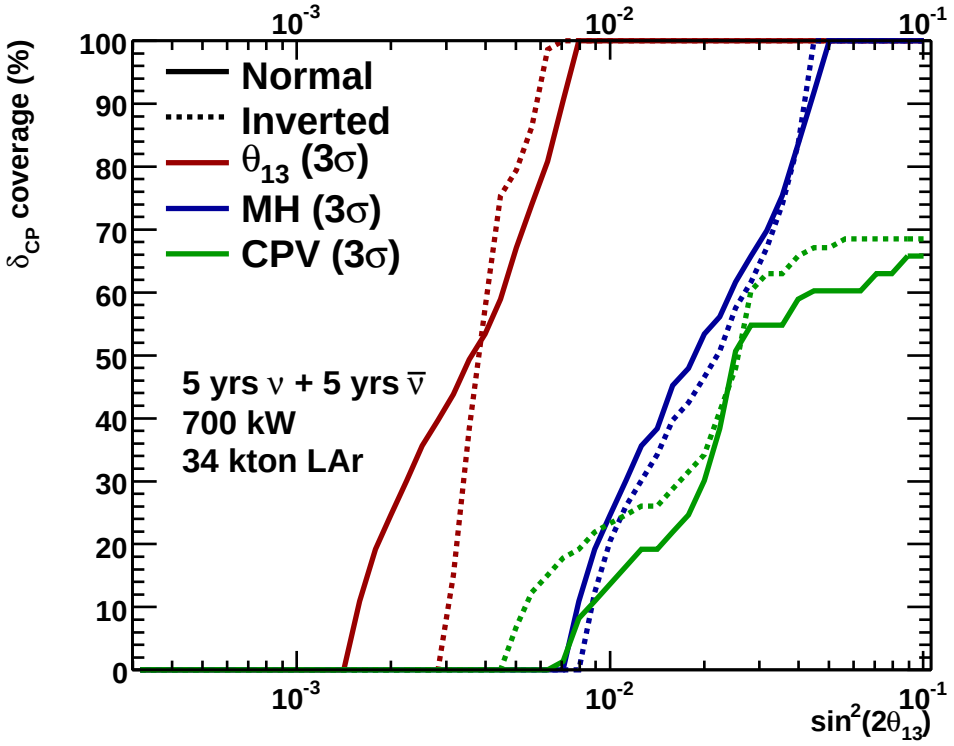

Figure 6–9: The fraction of δ_{cp} values for which a 3 σ resolution of the mass ordering (hierarchy) and determination of whether CP is violated ($\delta_{cp} \neq 0$ or π can be achieved by a 34 kton fiducial volume LArTPC for 5+5 yrs ($\nu + \bar{\nu}$) running in a 700kW beam.

FD is shown for different values of Δm^2_{32} and $\sin^2 2\theta_{23}$ for neutrinos and antineutrinos. A $\nu_\mu/\bar{\nu_\mu}$ CC reconstruction efficiency of 85% and a NC contamination rate of 0.5% is assumed for these measurements. The variation on the precision of the parameters for different values of the NC contamination is shown in Figure 6–13. The LAr-FD can achieve <1% precision on these parameters.

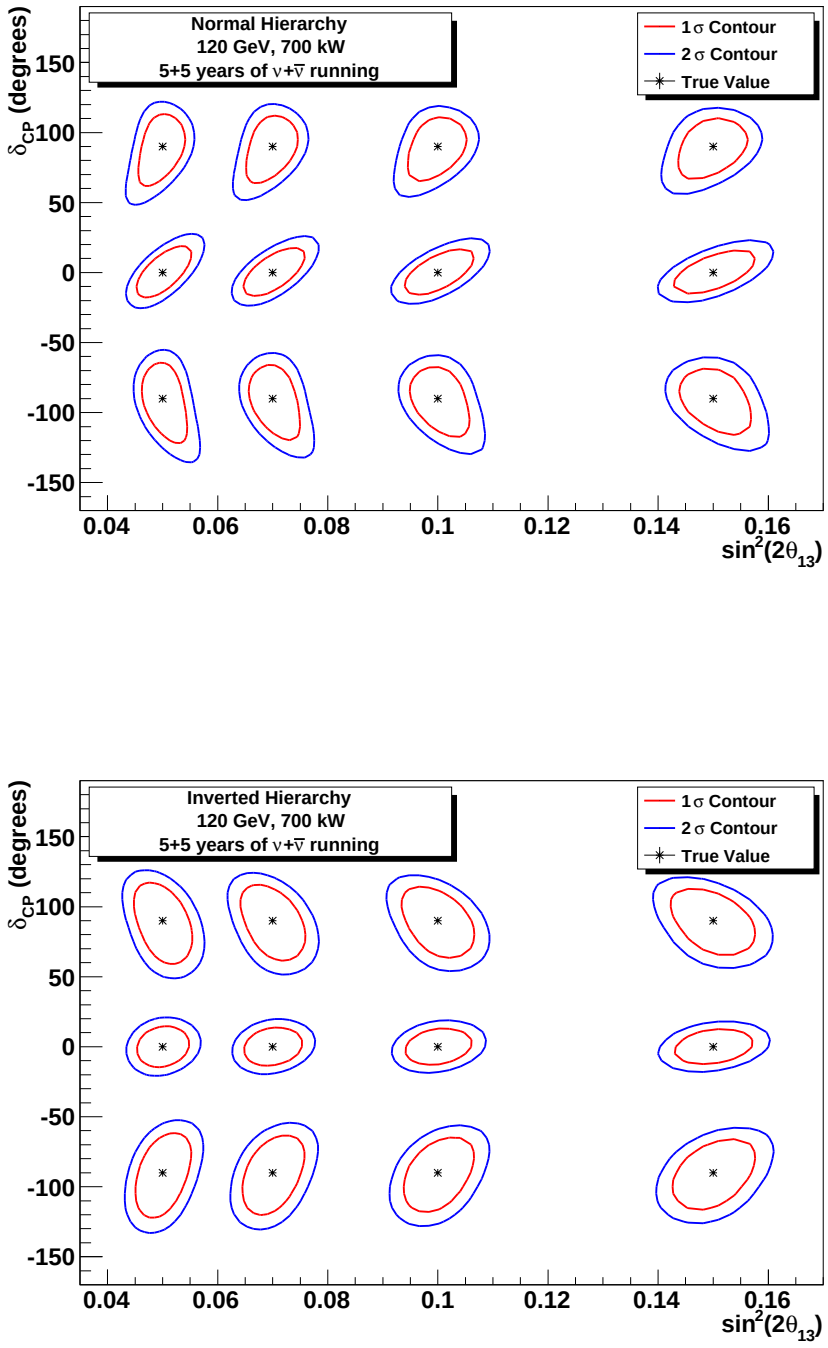

Figure 6–10: Fits to the values of $\sin^2 2\theta_{13}$ and δ_{cp} as a function of $\sin^2 2\theta_{13}$ for normal (top) and inverted (bottom) hierarchy.

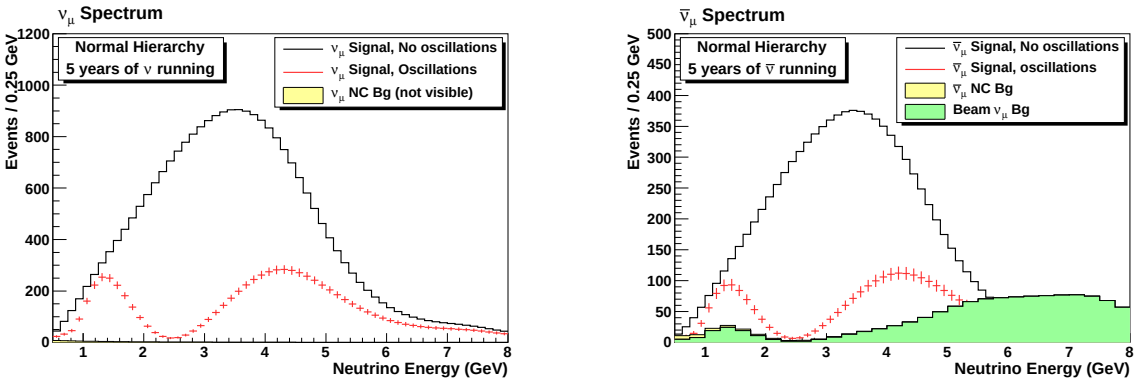

Figure 6–11: The expected spectrum of ν_μ or $\overline{\nu}_\mu$ events in a 34-kton LArTPC for five years of neutrino (left) and antineutrino (right) running with a 700 kW beam, with and without neutrino oscillation.

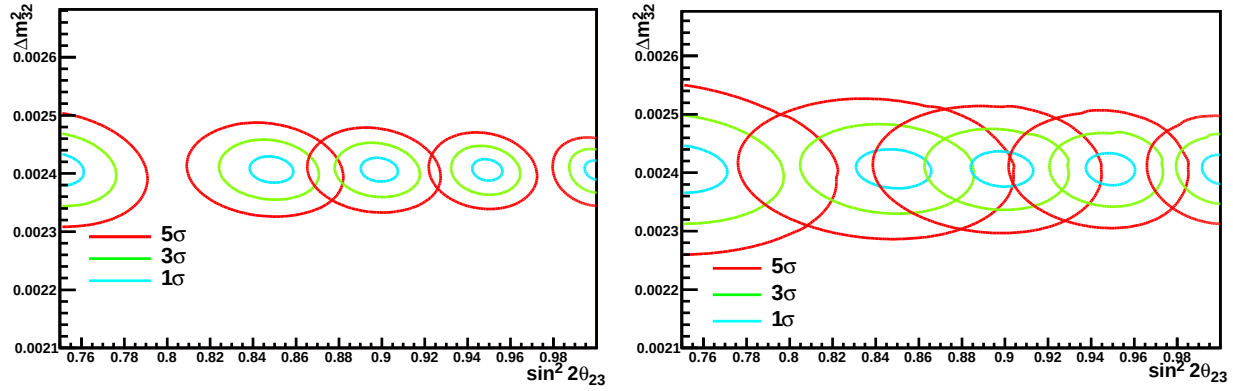

Figure 6–12: Fit to different values of Δm^2_{32} and $\sin^2 2\theta_{23}$, for neutrino running (left) and anti-neutrino running (right).

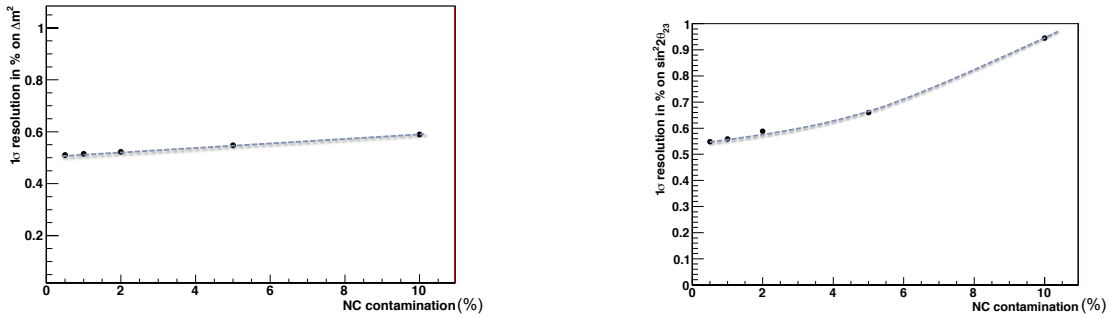

Figure 6–13: Impact of varying the NC contamination on the precision of measuring Δm^2_{32} (left) and $\sin^2 2\theta_{23}$ (right).

6.2.3 Observation of ν_τ Appearance

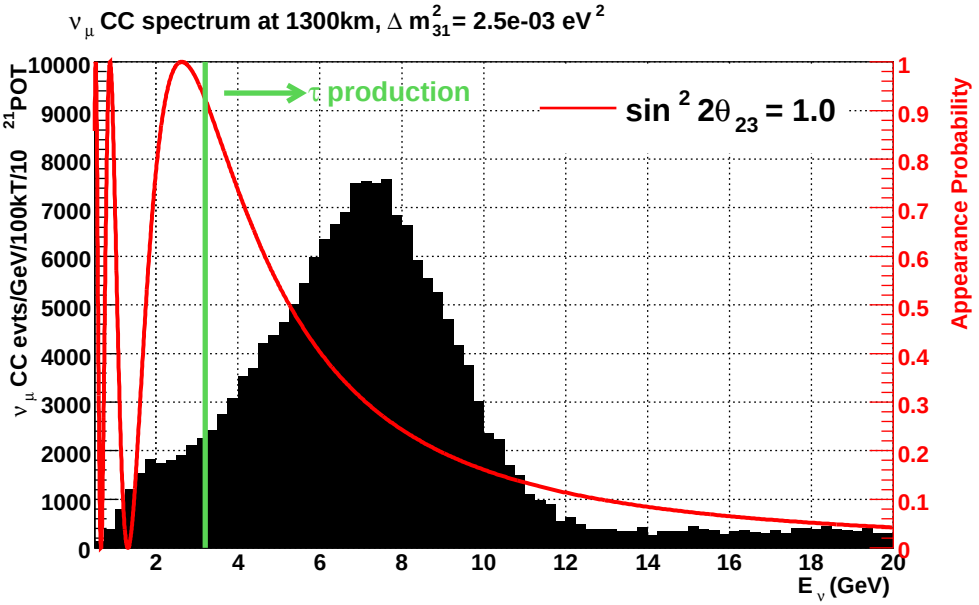

Figure 6–14: The $\nu_\mu \rightarrow \nu_\tau$ oscillation probability (red curve) at 1300km for $\sin^2 2\theta_{23} = 1.0$. The shaded histogram is the unoscillated ν_μ CC spectrum at 1300km from the medium-energy (ME) beam tune.

The LBNE baseline at 1,300 km will be longer than any long-baseline experiment currently in operation. As a result, ν_μ oscillations occur at higher energy and in particular the energy range is favorable to $\nu_\mu \rightarrow \nu_\tau$ appearance above the τ CC production threshold of 3.2 GeV, as shown in Figure 6–14. In this respect LBNE has a unique ability compared to current long-baseline experiments in that oscillation between all three flavors of neutrinos could be explicitly observed in a single experiment. To increase the ν_τ CC appearance signal, we are considering several high-energy beam tunes produced by moving the target further upstream of an updated design of LBNE horn 1.

In Table 6–1, ν_τ CC appearance rates for several LBNE beam tunes are shown. The first row in Table 6–1 corresponds to the baseline low-energy beam tune used for the primary oscillation physics. The last two rows correspond to two proposed high-energy beam tunes produced by pulling the target back by 1.5 m and 2.5 m from a double parabolic horn 1. The higher-energy beam tunes can be used to greatly enhance the ν_τ appearance rate. In particular, the medium-energy (ME) tune has high appearance rates for ν_e and ν_τ. It is to be noted that the OPERA-tau experiment which has seen one ν_τ CC interaction [21] expects a rate of two ν_τ events/1.25 kton/year compared to LBNE which would record a rate of 150 ν_τ events/34 kton/year in the ME beam.

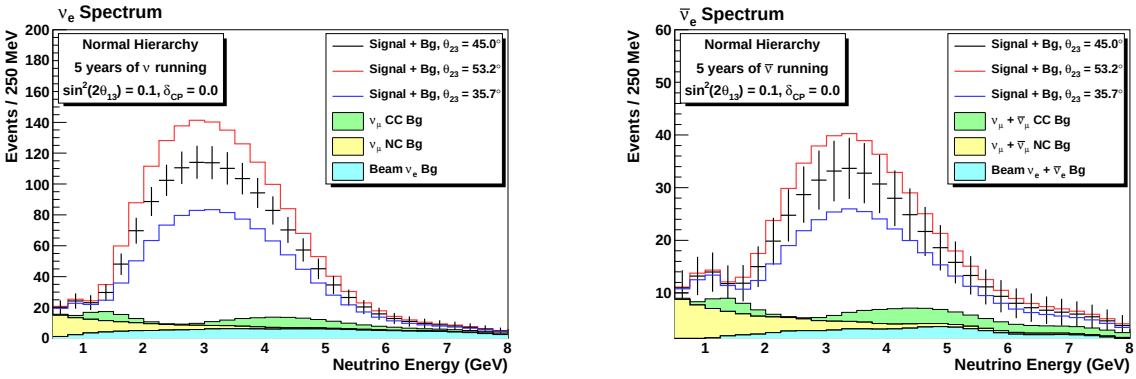

Figure 6–15: The expected spectrum of ν_e or $\overline{\nu}_e$ oscillation events in a 34-kton LArTPC for 5 years of neutrino (left) and antineutrino (right) running with a 700 kW beam, assuming normal hierarchy, $sin^2(2\theta_{13}) = 0.1, \delta_{cp} = 0$ and varying the value of θ_{23} within the current range of allowed values. Backgrounds are displayed as stacked histograms.

6.2.4 Resolving the θ_{23} octant

Current experimental results indicate that $\sin^2 2\theta_{23}$ is near maximal ($\sin^2 \theta_{23} > 0.91$ at 90% CL [22]), however there exist two solutions of θ_{23} for a given set of measured oscillation parameters, known as the θ_{23} *octant ambiguity*. If the oscillation associated with ν_μ disappearance is not maximal, then it will be important to determine whether θ_{23} is greater than or less than $\pi/4$. This in turn will help show whether the third neutrino mass eigenstate couples more strongly to ν_μ or ν_τ. The value of θ_{23} varies the $\nu_\mu \rightarrow \nu_e$ appearance spectrum as shown in Figure 6–15. The impact of the θ_{23} octant in the energy regions around the second oscillation maximum is very small compared to the effect of δ_{cp} – which is much larger at lower energies – and is the same for neutrinos and antineutrinos, which helps to resolve the degeneracy with the mass hierarchy and δ_{cp} in the region of the first oscillation maximum.

Figure 6–16 displays the capability of LBNE to resolve the θ_{23} octant with the 34 kton LAr-FD. Running in a 708 kW beam, LBNE is able to resolve the θ_{23} octant degeneracy for θ_{23} values less than 40° at 90% CL and 90% of δ_{CP} values if $\sin^2 2\theta_{13}$ is greater than 0.075 for 34 ktons of LAr. Improvements in the resolving power of LBNE could be achieved with more neutrino flux at lower energies to break degeneracies with δ_{cp} values.

6.2.5 Searches for New Physics in Long-Baseline Oscillations

In addition to precision measurements of the standard three-flavor neutrino oscillation parameters, LBNE is also well-suited for new physics searches in the neutrino sector. For

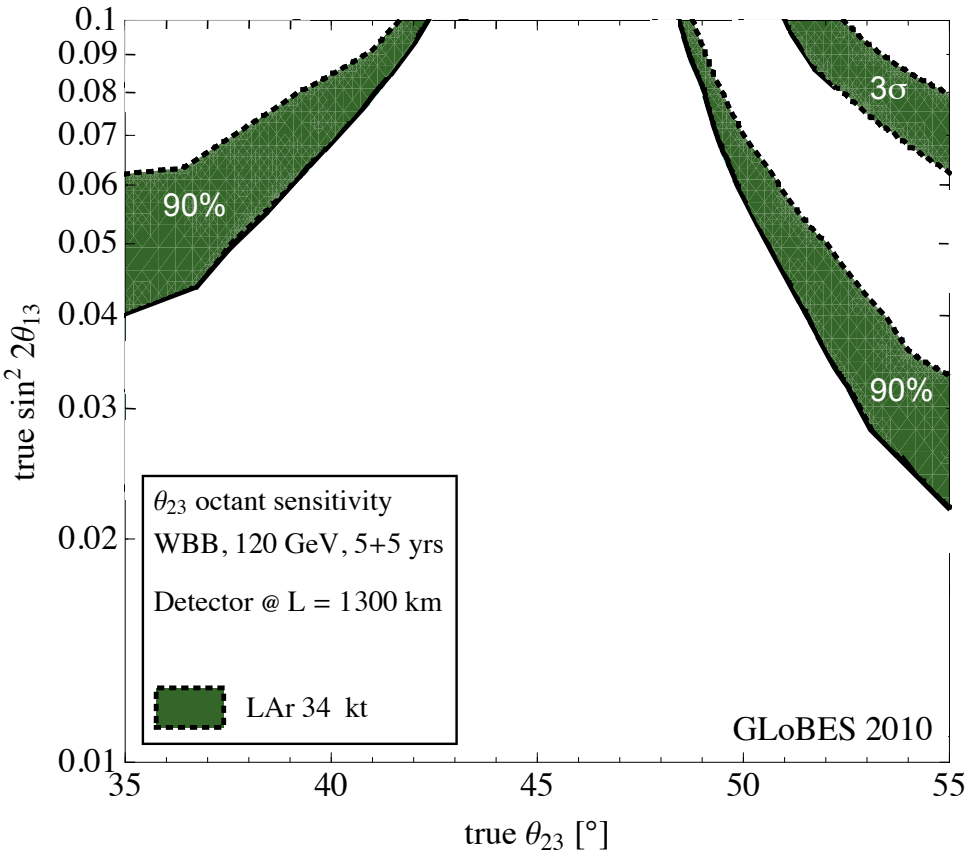

Figure 6–16: Sensitivity of LBNE to resolve the θ_{23} octant degeneracy for 5+5 years of ν+$\bar{\nu}$ running at 700 kW and normal mass hierarchy. The green band shows the results for 34 kton LAr. The width of the bands corresponds to the impact of different true values for δ_{CP}, ranging from a 10% to 90% fraction of δ_{CP}. In the region above the bands, the determination of the θ_{23} octant is possible at 90% CL (lower bands) and 3σ (upper bands).

example, the experiment is sensitive to non-standard neutrino interactions and active-sterile neutrino mixing, provided that these effects are not too weak.

6.2.5.1 Non-standard Interactions

NC non-standard interactions (NSI) can be understood as non-standard matter effects that are visible only in a far detector at a sufficiently long baseline. This is where LBNE has a unique advantage compared to other long-baseline experiments (except atmospheric neutrino experiments, which are, however, limited by systematic effects). NC NSI can be parameterized as new contributions to the MSW matrix in the neutrino-propagation Hamiltonian:

$$H = U \begin{pmatrix} 0 & & \\ & \Delta m^2_{21}/2E & \\ & & \Delta m^2_{31}/2E \end{pmatrix} U^\dagger + \tilde{V}_{\rm MSW}\,, \tag{6.1}$$

with

$$\tilde{V}_{\rm MSW} = \sqrt{2} G_F N_e \begin{pmatrix} 1+\epsilon^m_{ee} & \epsilon^m_{e\mu} & \epsilon^m_{e\tau} \\ \epsilon^{m*}_{e\mu} & \epsilon^m_{\mu\mu} & \epsilon^m_{\mu\tau} \\ \epsilon^{m*}_{e\tau} & \epsilon^{m*}_{\mu\tau} & \epsilon^m_{\tau\tau} \end{pmatrix} \tag{6.2}$$

Here, U is the leptonic mixing matrix, and the ϵ-parameters give the magnitude of the NSI relative to standard weak interactions. For new physics scales of few $\times$ 100 GeV, we expect $|\epsilon| \lesssim 0.01$.

To assess the sensitivity of LBNE to NC NSI, the NSI discovery reach is defined in the following way: After simulating the expected event spectra, assuming given "true" values for the NSI parameters, one attempts a fit assuming no NSI. If the fit is incompatible with the simulated data at a given confidence level, one would say that the chosen "true" values of the NSI parameters are within the experimental discovery reach. Figure 6–17 shows the NSI discovery reach of LBNE for the case where only one of the $\epsilon^m_{\alpha\beta}$ parameters is non-negligible at a time [23].

It can be concluded from the figure that LBNE will be able to improve model-independent bounds on NSI in the e–μ sector by a factor of two, and in the e–τ sectors by an order of magnitude.

6.2.5.2 Long-Range Interactions

The small scale of neutrino-mass differences implies that minute differences in the interactions of neutrinos and antineutrinos with background sources can be detected through perturbations to the time evolution of the flavor eigenstates. The longer the experimental baseline, the higher the sensitivity to a new long-distance potential acting on neutrinos. For example, some of the models for such long-range interactions (LRI) as described in [27] could contain discrete symmetries that stabilize the proton and a dark matter particle and thus provide new connections between neutrino, proton decay and dark matter experiments. The longer baseline of LBNE coupled with the expected precision of better than 1% on the ν_μ and $\bar{\nu}_\mu$ oscillation parameters improves the sensitivity to LRI beyond that possible by the current generation of long-baseline neutrino experiments.

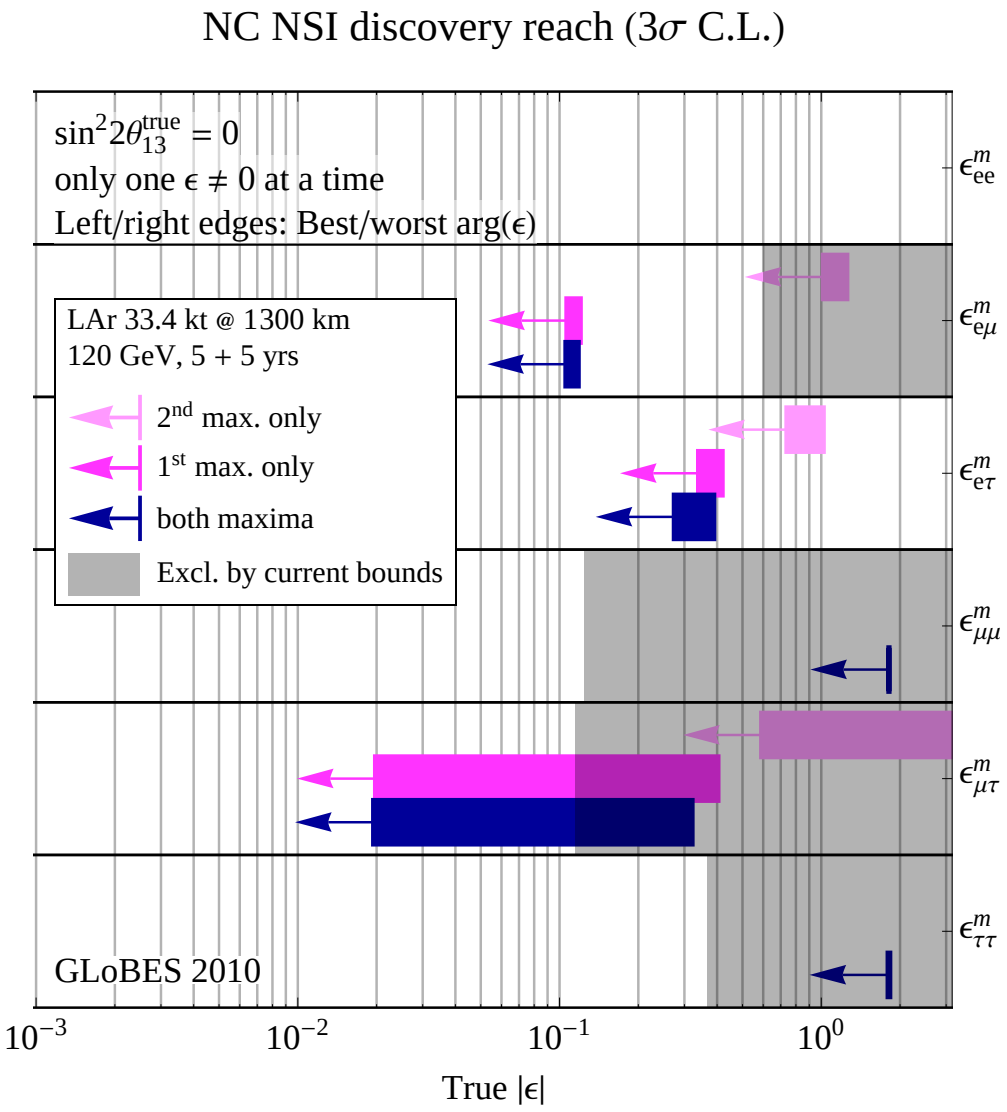

Figure 6–17: Non-standard interaction discovery reach in LAr-TPC. The left and right edges of the error bars correspond to the most favorable and the most unfavorable values for the complex phase of the respective NSI parameters. Red arrows indicate the current model-independent limits on the different parameters at 3 σ [24,25,26].

6.2.5.3 Search for Active-Sterile Neutrino Mixing

Searches for evidence of active sterile neutrino mixing at LBNE can be conducted by examining the NC event rate at the Far Detector and comparing it to a precision measurement of the expected rate from the Near Detector. Observed deficits in the NC rate could be evidence for active sterile neutrino mixing. The latest such search in a long baseline experiment was conducted by the MINOS experiment [28]. The expected rate of NC interactions with visible energy > 0.5 GeV in LBNE is approximately 5K events over five years (see Table 6–1). The NC identification efficiency is high with a low rate of ν_μ CC background mis-identification as shown in Table 6–2. LBNE will provide a unique opportunity to revisit this search with higher precision over a large range of neutrino energies.

6.3 Searches for Baryon Number Non-Conservation

Proton decay, and similar processes such as neutron-antineutron oscillation, test conservation of baryon number. Non-conservation of baryon number has never been observed; while it is predicted by many grand unified theories, it is not allowed in the Standard Model. For this reason, even a single detected event would be evidence of physics beyond the Standard Model and would strongly support the idea of grand unification.

6.3.1 Proton Decay

Figure 6–18 shows experimental limits on proton decay, dominated by recent results from Super–Kamiokande, compared to the ranges of lifetimes predicted by an assortment of GUTs. From the body of literature, two decay modes emerge that dominate experimental designs. First, there is the decay mode of $p \to e^+\pi^0$ that arises from gauge mediation. This is the most famous proton decay mode, often predicted to have the highest branching fraction, and also demonstrably the most straightforward experimental signature. The total mass of the proton is converted into the electromagnetic shower energy of the positron and the two photons from π^0 decay, with a net momentum vector near zero. The second key mode is $p \to K^+\nu$. This mode is dominant in most supersymmetric-GUTs, which also often favor several other modes involving kaons in the final state. This is due to the simple fact that the interaction would proceed via SUSY-Higgs exchange, which couples most strongly to quarks with the largest mass. The strange quark is the heaviest one with mass less than the nucleon mass.

The expected efficiency and background rates for the main experimental proton decay modes are summarized in Table 6–6. For $p \to e^+\pi^0$, an LArTPC of fiducial mass 34 ktons makes no improvement over the projected Super–Kamiokande limit by itself.

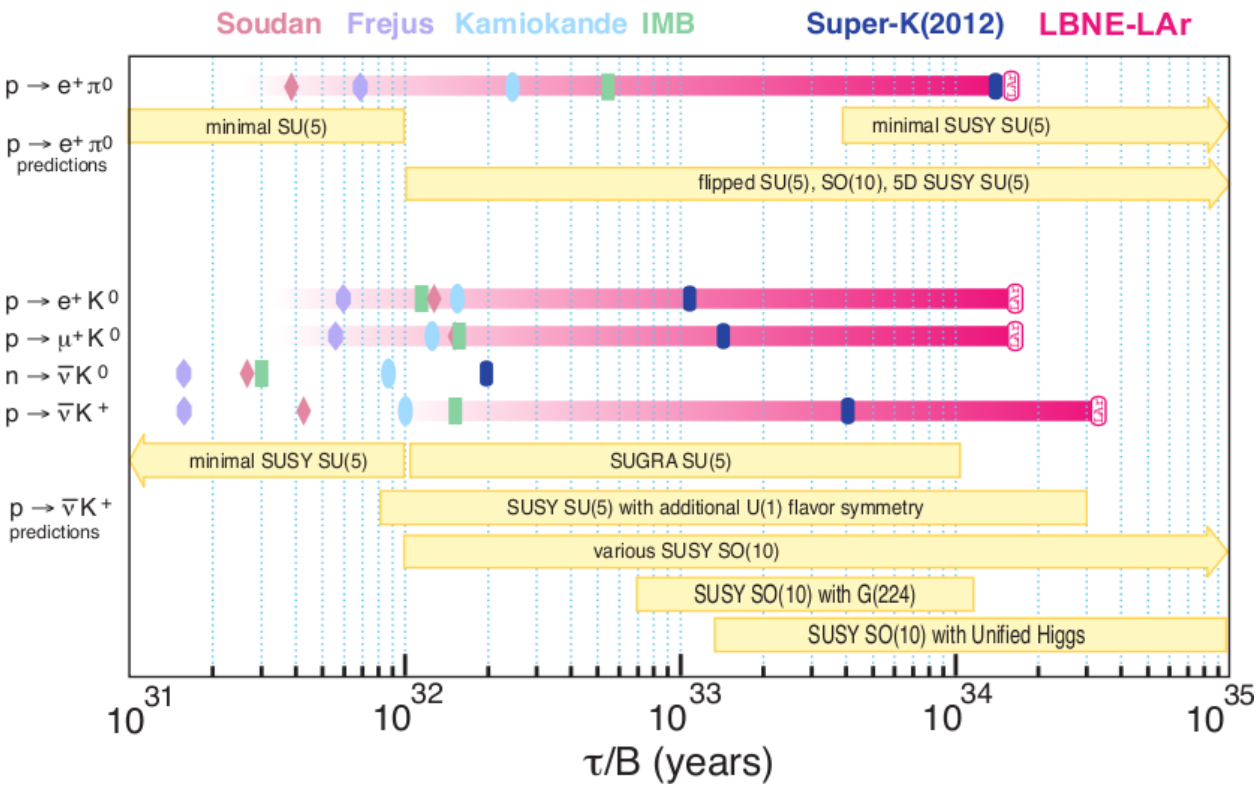

Figure 6–18: Proton decay lifetime limits compared to lifetime ranges predicted by Grand Unified Theories. The upper section is for $p \to e^+\pi^0$, most commonly caused by gauge mediation. The lower section is for SUSY motivated models, which commonly predict decay modes with kaons in the final state. The marker symbols indicate published limits by experiments, as indicated by the sequence and colors on top of the figure. The expected limits for 10 live years of 34 ktons of LAr are shown as bands terminating in an open symbol.

Mode	Efficiency	Background Rate (evts/100 kton-y)
B-L		
$p \to e^+\pi^0$	45%	0.1
$p \to \bar{\nu}K^+$	97%	0.1
$p \to \mu^+K^0$	47%	< 0.2
B+L		
$p \to \mu^-\pi^+K^+$	97%	0.1
$p \to e^+K^+$	96%	< 0.2
$\Delta B = 2$		
$N\bar{N} \to n(\pi)$	TBD	TBD

Table 6–6: Liquid argon efficiency and background numbers used for proton decay sensitivity calculations obtained from the paper by Bueno *et al.* [29].

LBNE will have a unique sensitivity to $p \to K^+\bar{\nu}$. The event signature is highly described by an LArTPC because the momentum of the kaon will result in a high-ionization density which can be compared to the range of the kaon. In addition, the charged kaon decays at rest to fully reconstructible final states, so high signal efficiency with low background is possible. Figure 6–19 shows a LArSoft [12] simulation of a K^+ decay. Reference [29] finds that an LArTPC has 97% detection efficiency for this mode, with a background rate of 0.1 events/100 kton-year.

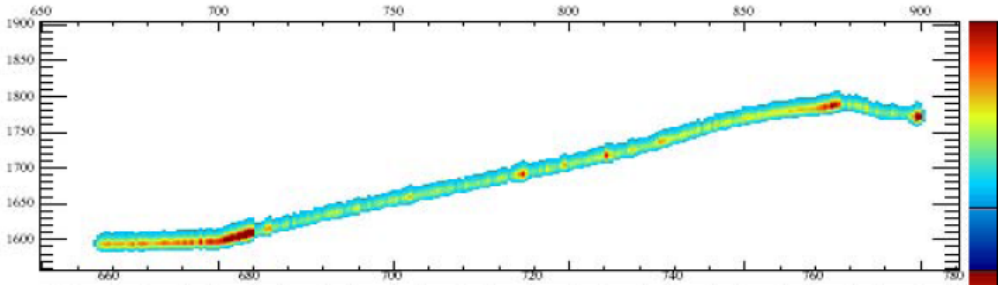

Figure 6–19: LArSoft simulation of $K^+ \to \mu^+ \to e^+$ decay in the MicroBooNE geometry. The drift time is along the vertical axis. The wire number is along the horizontal axis (3-mm wire spacing).

The most serious background to $p \to K^+\bar{\nu}$ is from cosmogenic neutral kaons undergoing charge-exchange in the detector. The overburden at the 4850L reduces this background to acceptable levels. Another background to $p \to K^+\bar{\nu}$ could result from misidentified atmospheric pions. For this reason, the ability to differentiate between kaons, pions, and muons in the LAr-FD is important for sensitivity to proton decay. Figure 6–1 shows the particle-identification capabilities of an LArTPC.

Figure 6–20 shows the proton-decay lifetime limit as a function of time for $p \to K^+\bar{\nu}$ for Super–Kamiokande and LBNE. The LAr-FD can produce significant improvement to the proton-lifetime limit for $p \to K^+\bar{\nu}$.

6.3.2 Neutron-Antineutron Oscillations

Neutron anti-neutron ($n\overline{n}$) oscillations violate only baryon number ($\Delta B = 2$), and are sensitive to new physics well below the GUT scale. These oscillations have been studied with free neutrons from nuclear reactors, with a best lifetime limit of 10^8 seconds from the ILL experiment [30] in Grenoble. The oscillation time of a bound neutron is suppressed by the nuclear potential of the nucleus, but may be compared to the free-neutron lifetime. The signature is the appearance of two to six pions with zero net momentum and total energy of roughly 2 GeV. An example of such a signature in an LAr-TPC is shown in Figure 6–21. The current best limit is by Super–Kamiokande [31], with a bound lifetime greater than 2×10^{32} years, corresponding to a free lifetime greater than 2×10^8 seconds. The Super–Kamiokande

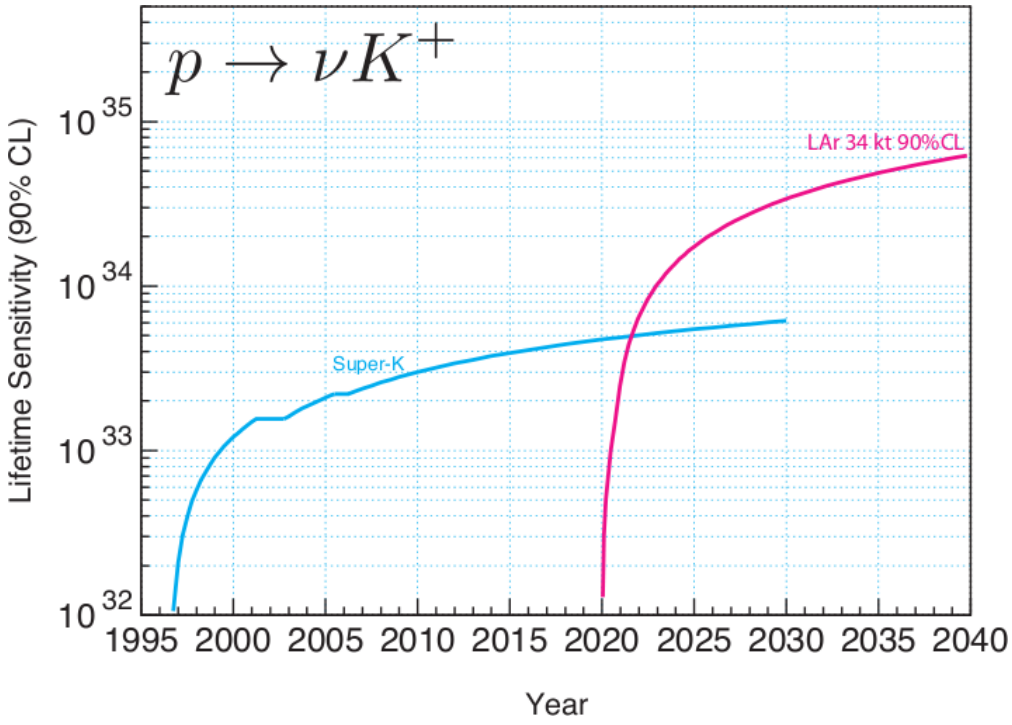

Figure 6–20: Proton decay lifetime limit for $p \to K^+\bar{\nu}$ as a function of time for Super-Kamiokande compared to the 34 kton fiducial LAr-FD at the 4850 level starting in 2020. The limits are at 90% C.L., calculated for a poisson process including background assuming the detected events equals the expected background.

result is seriously background limited with a rate in the present analysis of 27 events per 100 kton years exposure, and a detection efficiency of only 12%. The dominant background is atmospheric neutrinos and the experimental difficulty is the inability of water Cherenkov detectors to observe low-momentum charged pions. The ability of the LAr detector to resolve low-momentum pions, as well as gamma showers from π^0 decay, combined with the ability to reject atmospheric-neutrino interactions with recoil protons and charged-current leptons, should enable a low-background search for neutron antineutron annihilation in the argon nucleus.

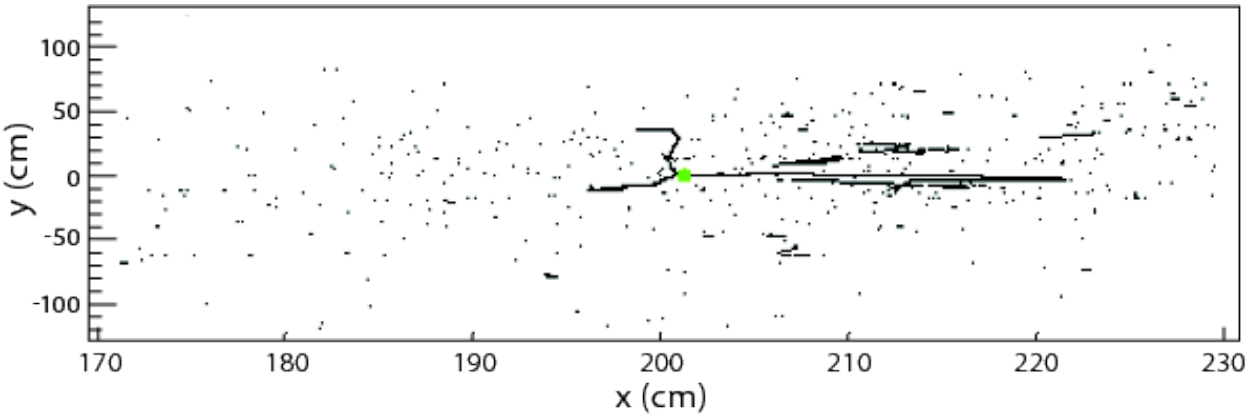

Figure 6–21: LArSoft simulated event, $p\bar{p}$ annihilation at rest

6.4 Supernova-Burst Neutrinos

If a core-collape supernova occurs in our galaxy during the lifetime of LBNE, the LAr-FD will detect the associated burst of neutrinos. The explosion mechanism is thought to have three distinct stages: the collapse of the iron core, with the formation of the shock and its breakout through the neutrinosphere; the accretion phase, in which the shock temporarily stalls at the radius of about 200 km, while the material keeps raining in; and the cooling stage, in which the hot proto-neutron star loses its energy and trapped lepton number, while the re-energized shock expands to push out the rest of the star. All these stages are predicted to have distinct signatures in the neutrino signal. Thus, it should be possible to directly observe, for example, how long the shock is stalled. More exotic features of the collapse may be observable in the neutrino flux as well, such as possible transitions to quark matter or to a black hole. (An observation in conjunction with a gravitational wave detection would be especially interesting.)

Supernova neutrinos are emitted in a few tens of seconds duration, with about half in the first second, they have energies of a few tens of MeV, and their luminosity is divided roughly equally between the three neutrino flavors. In addition to shedding light on the explosion mechanisms of the supernova, the detection of supernova-burst neutrinos would allow for a wealth of neutrino-oscillation physics measurements ranging from independent determination

of the neutrino mass hierarchy to the equation of state of matter at nuclear densities, to constraints on physics beyond the Standard Model. Neutrinos from a core collapse arrive earlier than electromagnetic radiation; the detection of a neutrino signal would provide an alert for astronomers, allowing the observation of light-curves in early stages of the supernova. The expected rate of core-collape supernovae in the Milky Way is 2–3 per year; in a 20-year lifetime, there is a 40% chance for LBNE to observe such an event.

The sensitivity to physics associated with a supernova burst is determined by the total detector mass. Figure 6–22 shows the neutrino event rates as function of observed energy for a 34-kton fiducial LArTPC using the Livermore model [32] of supernova-neutrino flux. Table 6–7 lists the event rates predicted by both the Livermore model and the "GKVM" model [33]. The primary sensitivity is to the ν_e component.

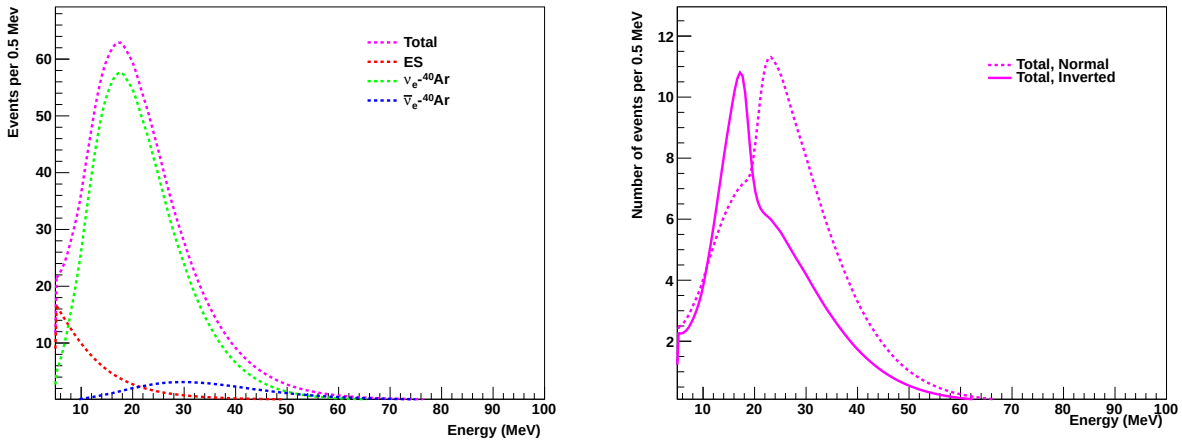

Figure 6–22: Event rates (per 0.5 MeV) in a 34-kton LArTPC as a function of observed energy for the Livermore model [32] of supernova neutrino flux (left), and comparison of total event rates (per 0.5 MeV) for normal and inverted hierarchies, for a late-time slice of a different flux model in a 34-kton LAr module (right).

Channel	Events, "Livermore" model	Events, "GKVM" model
$\nu_e + ^{40}\mathrm{Ar} \rightarrow e^- + ^{40}\mathrm{K}^*$	2308	2848
$\bar{\nu}_e + ^{40}\mathrm{Ar} \rightarrow e^+ + ^{40}\mathrm{Cl}^*$	194	134
$\nu_x + e^- \rightarrow \nu_x + e^-$	296	178
Total	2794	3160

Table 6–7: Supernova burst neutrino event rates for different models in 34 kton of LAr.

Figure 6–22 also compares event rates for normal and inverted hierarchies in a 34-kton LArTPC, for a late-time slice of the ν_e spectrum in a particular flux model. The difference between the hierarchies is quite dramatic.

Initial estimates of cosmogenic backgrounds to the signal of supernova neutrinos in an LAr detector at the Sanford Laboratory are documented in reference [34]. The location at the 4850L will significantly reduce the background level and backgrounds in the LArTPC will be well-characterized and can be statistically subtracted from the burst signal.

6.5 Atmospheric Neutrinos

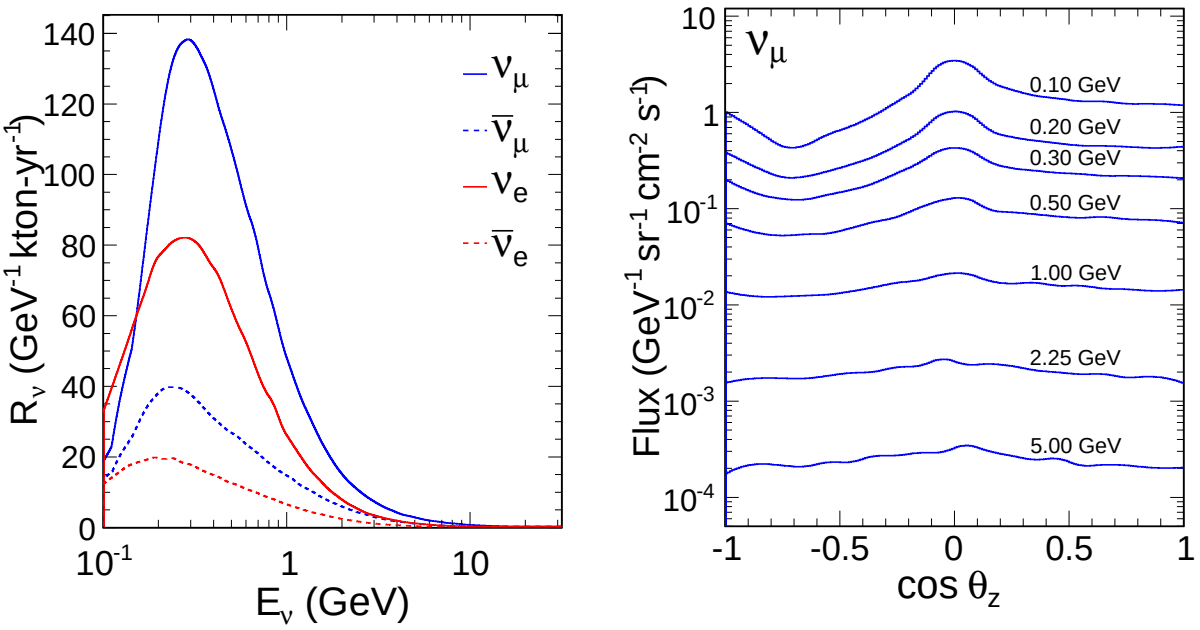

Figure 6–23: The expected atmospheric neutrino event rate obtained from the Bartol model at solar maximum. The energy spectrum of atmospheric neutrinos for different species is shown on the left and the angular distribution of the ν_μ flux is shown on the right.

Atmospheric neutrinos are unique among sources used to study oscillations: the oscillated flux contains neutrinos and antineutrinos of all flavors, and matter effects play a significant role. Since the oscillation phenomenology plays out over several decades in energy (see Figure 6–24) and path length, atmospheric neutrinos are very sensitive to alternative explanations or subdominant new physics effects that predict something other than the characteristic (L/E) dependence predicted by oscillations in the presence of matter. This power has already been exploited by the Super-Kamiokande in fits that compare their data binned in terms of energy and zenith angle to a host of new physics including CPT violation [35,36], Lorentz invariance violation [37,38], non-standard interactions [39], Mass Varying Neutrinos (MaVaNs) [40], and sterile neutrinos [41,42,43]. In numerous cases the best limits on exotic scenarios comes from the atmospheric neutrino analysis.

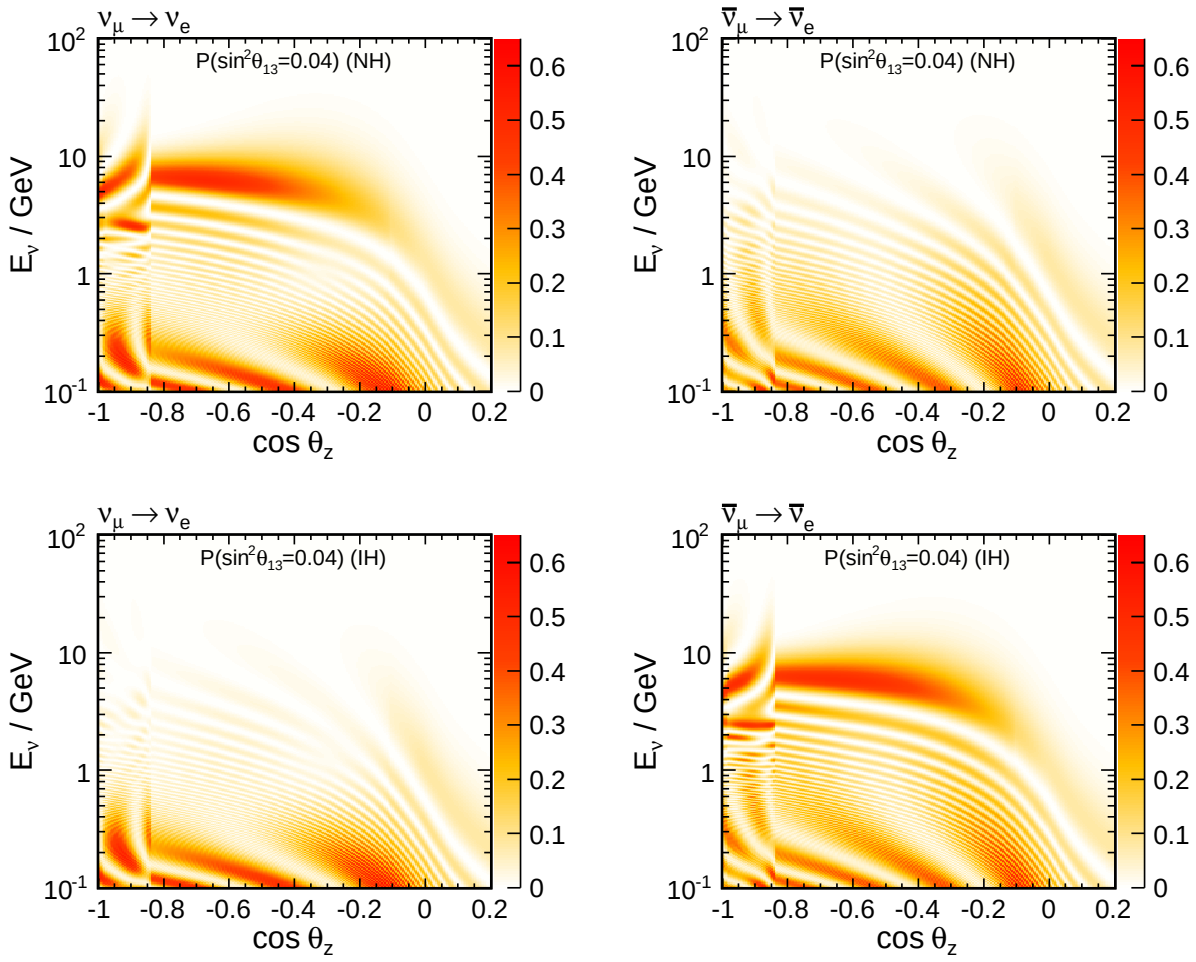

Figure 6–24: Atmospheric $\nu_\mu \rightarrow \nu_e$ oscillations vs energy and zenith angle for normal hierarchy (top) and inverted hierarchy (bottom). The z axis is the oscillation probability for $\sin^2(2\theta_{13}) = 0.15$.

The excellent CC/NC separation and the ability to fully reconstruct the hadronic final state in CC interactions in an LArTPC would enable the atmospheric neutrino 4-momentum to be fully reconstructed. This would enable a higher-resolution measurement of L/E to be extracted from atmospheric-neutrino events in an LArTPC compared to the measurements obtained from Super-Kamiokande. Using the expected range of performance parameters for the LAr-FD as summarized in Table 6–2, the zenith angle distribution of atmospheric neutrinos of different flavors in a 17-kton fiducial LAr-FD module and five years of running is shown in Figure 6–25. The atmospheric neutrino flux obtained from the Bartol model as shown in Figure 6–23, and the GENIE cross sections on an LAr target are used to model atmospheric-neutrino interactions in the LBNE LAr-FD. The expected interaction rate is 285 events per kton-year.

LBNE will be able to resolve the mass hierarchy using atmospheric neutrinos alone with

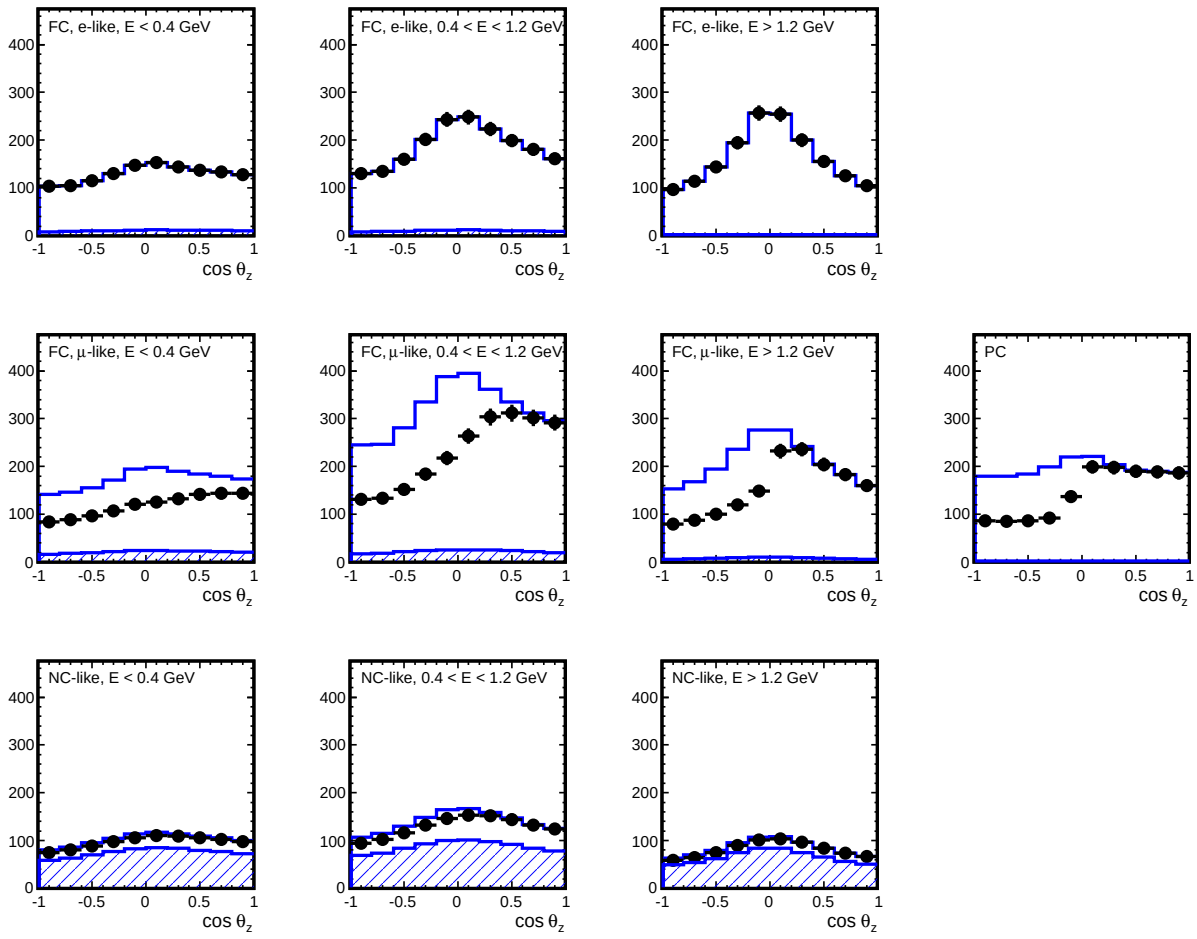

Figure 6–25: Zenith angle distribution for LBNE atmospheric neutrinos in a LAr-TPC with a mass of 20 ktons (17 ktons fiducial) and an exposure of 5 years. The solid line is for no oscillations, the hatched region is the true NC component, and the points are the oscillated expectation with some Poisson error bars added. The top set of plots is for ν_e CC interactions, the middle plots are for ν_μ CC interactions and the bottom set of plots are for NC interactions. The events are divided into several energy bins as well as identified by containment: fully contained (FC) and partially contained (PC).

$> 99\%$ C.L. after ten years of running with a 34-kton fiducial LArTPC for values of $\sin^2\theta_{13} > 0.03$. In addition, atmospheric neutrinos provide an independent constraint on the θ_{23} octant from the sub-dominant oscillation at the solar mass scale – regardless of the value of θ_{13}. The sensitivities to the mass hierarchy and the octant of θ_{23} obtained from atmospheric neutrinos alone are shown in Figure 6–26.

In addition to the oscillation studies of atmospheric ν_μ, ν_e CC and ν NC, a 34-kton LArTPC will observe a significant excess of ν_τ CC events. A set of simple cuts on visible energy, reconstruction zenith angle and energy of the highest-energy pion in events lacking a charged

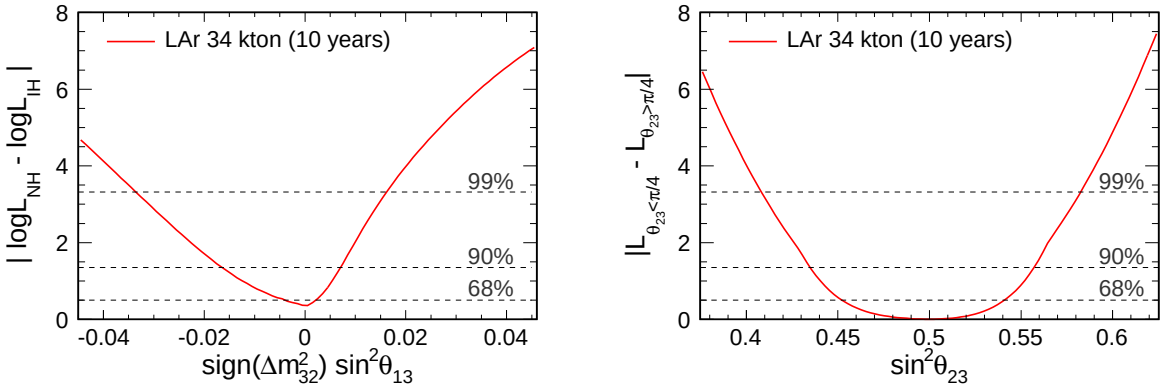

Figure 6–26: Sensitivities to the mass hierarchy as a function of the value of $sin^2\theta_{13}$ (left) and the θ_{23} octant (right) from atmospheric neutrinos in a LAr-TPC with 34 kton fiducial mass and 10 yrs of running. These sensitivities are estimated using statistical uncertainties only.

lepton, a 4.3 σ excess over background can be identified in a 100-kton-year exposure [44]. Confirmation of the appearance of tau neutrinos at the expected level in the atmospheric-neutrino flux as well as in the beam neutrinos will be an important consistency check on our overall oscillation picture.

6.6 Accelerator-based Short-Baseline Neutrino Oscillations

The primary purpose of the LBNE Near Detectors is to minimize systematic uncertainties present in the analysis of the Far Detector data and provide a detailed prediction of the un-oscillated neutrino flux measurement at the Far Detector. In Volume 3, Chapter 4 of this CDR, the strategy with which to carry out such measurements is discussed. The reference design for the near neutrino detector (ND) is a liquid argon TPC tracker (LArTPCT). The LArTPCT will be magnetized and the performance parameters are assumed to be similar to those of the LAr-FD.

An alternate design under considerations is a straw-tube fine-grained tracker (FGT). The FGT is composed of a straw-tube tracker (STT), with transition-radiation detection capability, surrounded by a 4π electromagnetic calorimeter, inside a dipole magnetic field of B $\approx$ 0.4 T. The tracker will have argon-gas in pressurized tubes as the neutrino target. Detectors to identify muons are placed within the magnet yoke as well as at downstream, and outside, of the magnet. There is currently no detailed GEANT simulation of the LBNE Near Detector FGT. However, the sensitivity to different measurements is based on the performance and results achieved by NOMAD [45] which forms the basis for the straw tube option of the FGT.

The two ND designs under consideration are very high-resolution magnetized tracking de-

tectors that are placed in a short-baseline, high-intensity neutrino beam. The LBNE ND is coupled with the next-generation instrumentation of the neutrino beam (Volume 3, Chapter 3 of this CDR) that would enable an independent measurement of the neutrino flux expected at the ND. The combination of neutrino-beam measurements, a high-intensity beam and high-resolution neutrino detectors enables LBNE to carry out a rich program of short-baseline neutrino physics. Estimated ν_μ production rates on argon at the near ND location are shown in Table 6–8.

Table 6–8: Estimated ν_μ production rates in an argon target per ton for 1×10^{20} POT at 459 m assuming neutrino cross section predictions from NUANCE [46] and a 120-GeV proton beam, 250-kA horn current, and a 2-m radius 250-m long decay region. Processes are defined at the initial neutrino interaction vertex and thus do not include final state effects. These estimates do not include detector efficiencies or acceptance [47,48].

Production mode	Rate/ton of Ar
CC QE ($\nu_\mu n \to \mu^- p$)	50K
NC elastic ($\nu_\mu N \to \nu_\mu N$)	18K
CC resonant π^+ ($\nu_\mu N \to \mu^- N \pi^+$)	68K
CC resonant π^0 ($\nu_\mu n \to \mu^- \, p \, \pi^0$)	16K
NC resonant π^0 ($\nu_\mu N \to \nu_\mu \, N \, \pi^0$)	16K
NC resonant π^+ ($\nu_\mu p \to \nu_\mu \, n \, \pi^+$)	6.9K
NC resonant π^- ($\nu_\mu n \to \nu_\mu \, p \, \pi^-$)	6.0K
CC DIS ($\nu_\mu N \to \mu^- X$, $W > 2$)	69K
NC DIS ($\nu_\mu N \to \nu_\mu X$, $W > 2$)	24K
CC coherent π^+ ($\nu_\mu A \to \mu^- A \pi^+$)	3.9K
NC coherent π^0 ($\nu_\mu A \to \nu_\mu A \pi^0$)	2.0K
NC resonant radiative decay ($N^* \to N\gamma$)	0.11K
Inverse Muon Decay ($\nu_\mu e \to \mu^- \nu_e$)	12
$\nu_\mu e^- \to \nu_\mu e^-$	29
Other	42.6K
Total CC	236K
Total NC+CC	322K

A summary of possible physics measurements that could be achieved by the LBNE ND is discussed here. More details on the LBNE short-baseline physics program can be found in the Fall 2010 Report from the LBNE Physics Working Group [6].

6.6.1 Absolute Flux Determination

The flux of neutrinos — both for signal and for background — is different at ND and FD, therefore, to conduct precise measurements of long baseline ν_μ oscillations, one needs to know the absolute neutrino cross-section, and hence, absolute neutrino flux, to about 3–5% precision in $0.5 \leq E_\nu \leq 10$ GeV. Absolute flux is necessary for precision measurements and

to determine sensitivity to new physics at the FD. The LBNE ND provides two independent, in situ determination of the absolute ν_μ flux.

The first method uses the elastic ν-electron NC scattering whose cross-section is known to $\simeq 1\%$ precision. The signal is characterized by a single e^- collinear with the beam. The background, dominated by quasi-exclusive π^0, where one of the photons converts asymmetrically and other evades detection, is charge symmetric. The known cross-section and the ν-e NC events then yield an absolute measure of the neutrino flux in the $0.5 \leq E_\nu \leq 10$ GeV range to $\simeq 2.5\%$ precision over a 5-year running. The second method uses the 'inverse muon decay' (IMD) signal, $\nu_\mu e^- \rightarrow \mu^- \nu_e$, with a very known cross-section, to determine the absolute flux in $E_\nu \geq 11$ GeV region. Both methods are statistics limited.

6.6.2 Detailed Studies of the Weak Interaction

A measurement of the weak mixing angle (WMA), $sin^2\theta_W$, with a precision approaching 0.2% remains a prized-jewel for any short-baseline neutrino program. NuTeV [49] has conducted the most precise determination of WMA which, however, is 3σ away from the expected value. One method of WMA determination uses the deep inelastic (anti)neutrino-nucleon NC and CC interactions with hadronic energy, E_{HAD}, greater than 3 GeV. LBNE offers several advantages over NuTeV, for example, (1) NC is identified as an event with a large missing transverse momentum but with no-muon; (2) ν_e and $\overline{\nu}_e$ are essentially not a background, (3) vertex resolution of either ND design is much, much better than that of a calorimeter. The disadvantage of LBNE with respect to NuTeV is the lower neutrino energy, but over the lifetime of LBNE we will have a high-energy run to constrain beam systematics which will also furnish a higher-energy spectrum for WMA analysis. In the baseline low-energy beam tune, there is expected to be a sufficient excess of NC events in LBNE in a five-year $\nu(\overline{\nu})$ running period, providing enough statistics to measure WMA to about 0.1% precision.

The LBNE NDC provides a unique matrix of measurements to explore the structure of the weak current to a precision no other experiment has attempted. Using the coherent π^0, π^+ and π^- interactions, the partially conserved vector current (PCAC) and the low-Q^2 structure of the weak current can be explored. The coherent-pion interactions would have a clean signature in LBNE where the backgrounds from QE, resonance and DIS channels can be precisely controlled. Using the coherent ρ^0, ρ^+, and ρ^- interactions, the conserved vector current (CVC) and the vector-hadron dominance (VMD) of the weak current can be explored. The coherent-ρ^+/ρ^- have been observed at $\simeq 3\sigma$ level, but coherent-ρ^0 has not been observed.

6.6.3 New Physics Searches with the Near Neutrino Detector

The LBNE near neutrino detector's ability to measure all four species of CC interactions, ν_μ-, $\overline{\nu}_\mu$-, ν_e- and $\overline{\nu}_e$-CC, permits a sensitive search for $\nu_\mu \rightarrow \nu_e$ transition, or, equivalently, oscillation with high-Δm^2 ($\geq$ 1eV^2). Using ν_μ- and $\overline{\nu}_\mu$-CC events, the electron-neutrino yields from μ and charged-kaons in the beam can be determined to a high precision. (Both NOMAD and NuTeV used this method to constrain the ν_e content of the beam.) Additionally, the K^0_L component can be uniquely determined using the small anti-ν_e in the beam, if sufficient charge separation of e^+/e^- can be achieved. Finally, the non-prompt background (dominated by NC) can be measured using kinematic variables in the plane transverse to the neutrino-direction. Preliminary studies with the FGT suggest that the probability of $\nu_\mu \rightarrow \nu_e$ transition can be explored with a sensitivity of 10^{-4}, i.e., an order of magnitude better precision than currently available.

Searches for $\nu_\mu \rightarrow \nu_\tau$ transitions due to CC non-standard interactions over short baselines can be carried out by the Near Detectors. The search for τ-appearance in both Near and Far Detectors is done using the existence of missing transverse momentum in the non-muonic decay modes. A combination of running with the higher-energy beam tunes and a high-resolution near neutrino detector will potentially allow the LBNE Near Detector to improve the sensitivity to $\nu_\mu \rightarrow \nu_\tau$ beyond what was achieved by NOMAD.

6.6.4 Studies of Nuclear and Nucleon Structure

Strange content of the nucleon, structure functions, perturbative versus non-perturbative QCD, strange meson and baryon production and sum-rules, among other sensitivity studies, are conducted by the LBNE Short-Baseline Physics (SBP) group. Some of these studies are summarized in [6].

6.7 Summary of Expected Measurements in LBNE

Table 6–9: Expected measurement precision/sensitivities of long-baseline ν_μ oscillation parameters in LBNE assuming an exposure of 34 kton LAr, 5+5 years $\nu + \bar{\nu}$ running at 708 kW. Values are quoted assuming a normal mass hierarchy.

Parameter	Resolution/Sensitivity
$\nu_\mu \to \nu_e$ CC	
Sign Δm^2_{31}	$> 5\sigma$ for all values of δ_{cp}
$\delta_{cp} \neq 0, \pi$	$> 3/5\sigma$ for 65%/40% of δ_{cp} values
$\sin^2 2\theta_{13} = 0.1$	$\sigma(\sin^2 2\theta_{13}) = 0.005$
$\delta_{CP} = 0$	$\sigma(\delta_{cp}) = 18^\circ$
Determination of θ_{23} quadrant	$> 90\%$ C.L. for $\theta_{23} < 42^\circ$ and $\theta_{23} > 49^\circ$
Non standard interactions	Figure 6–17
$\nu_\mu \to \nu_\mu$ CC	
$\sin^2 2\theta_{23} = 1.0$ (ν)	$\sigma = 0.007$
$\Delta m^2_{32} = 2.4 \times 10^{-3}$ eV^2 (ν)	$\sigma = 0.017 \times 10^{-3}$ eV^2
$\sin^2 2\theta_{23} = 1.0$ $(\bar{\nu})$	$\sigma = 0.011$
$\Delta m^2_{32} = 2.4 \times 10^{-3}$ eV^2 $(\bar{\nu})$	$\sigma = 0.025 \times 10^{-3}$ eV^2
Non standard interactions	Figure 6–17
Long range interactions α	ongoing studies
$\nu \to \nu$ NC	
Sterile fraction, f_s	ongoing studies
Non-standard interactions	ongoing studies
$\nu_\mu \to \nu_\tau$ CC	
ν_τ appearance	ongoing studies

Table 6–10: Expected measurement precision/sensitivities using short-baseline ν_μ interactions in the NDC, with an LAr and a 7 t FGT, assuming an exposure of 5+5 years $\nu + \bar{\nu}$ running at 708 kW.

Parameter	Resolution/Sensitivity
Absolute Flux	2.5–3%
$\sin^2 \theta_W$ using ν-q	$\to 0.25\%$
$\sin^2 \theta_W$ using ν-e	$\to 0.5\%$
P($\nu_\mu \to \nu_e$) ($\Delta m^2 \geq 1$ eV^2)	$\to 10^{-4}$
P($\nu_\mu \to \nu_\tau$) ($\Delta m^2 \geq 1$ eV^2)	$\to 10^{-5}$
PCAC (Coherent-π^0, π^+, π^-)	OK
CVC/VMD (Coherent-ρ^0, ρ^+, ρ^-)	OK

7 Supporting Documents

A host of information related to the CDR is available in a set of supporting documents. Detailed information on risk analysis and mitigation, value engineering, ES&H, costing, project management and other topics not directly in the design scope can be found in these documents, listed in Table 7–1. Each document is numbered and stored in LBNE's document database, accessible via a username/password combination provided by the Project. Project documents stored in this database are made available to internal and external review committees through Web sites developed to support individual reviews.

Table 7–1: LBNE CD-1 Documents

Title	**LBNE Doc Number(s)**
Acquisition Plan	5329
Alternatives Analysis	4382
Case Study Report; Liquid Argon TPC Detector	3600
Configuration Management Plan	5452
DOE Acquisition Strategy for LBNE	5442
Integrated Environment, Safety and Health Management Plan	4514
LAr-FD Preliminary ODH Analysis	2478
Global Science Objectives, Science Requirements and Traceback Reports	4772
Preliminary Hazard Analysis Report	4513
Preliminary Project Execution Plan	5443
Preliminary Security Vulnerability Assessment Report	4826
Project Management Plan	2453
Project Organization Chart	5449
Quality Assurance Plan	2449
Report on the Depth Requirements for a Massive Detector at Homestake	0034
Requirements, Beamline	4835
Requirements (Parameter Tables), Far Detector	3747 (2843)

Requirements, Far Site Conventional Facilities	4408
Requirements, Near Detectors	5579
Requirements, Near Site Conventional Facilities	5437
Risk Management Plan	5749
Value Engineering Report	3082
Work Breakdown Structure (WBS)	4219

References

[1] S.Amoruso *et al. Eur. Phys. J.*, vol. C33, p. 233, 2004.

[2] LBNE Science Collaboration, LBNE Case Study Report, Liquid Argon TPC Far Detector, Draft Version 1.2, October 2, 2011.

[3] F. An *et al.*, "The Theory of Neutrinos," 2005. arXiv:hep-ph/0510213v2.

[4] F. An *et al.*, "Observation of electron-antineutrino disappearance at Daya Bay," 2011. arXiv:1203.1669 [hep-ex].

[5] Particle Physics Project Prioritization Panel, "US Particle Physics: Scientific Opportunities; A Strategic Plan for the Next Ten Years," 2008. `http://science.energy.gov/~/media/hep/pdf/files/pdfs/p5_report_06022008.pdf`.

[6] T. Akiri *et al.*, "The 2010 Interim Report of the Long-Baseline Neutrino Experiment Collaboration Physics Working Groups." arXiv:1110.6249.

[7] LBNE Project Office, "LBNE Project Management Plan," tech. rep., FNAL, 2011. LBNE Doc 2453.

[8] LBNE Project Office, "Key Assumptions: Physics Research Goals of the LBNE Project," tech. rep., FNAL, 2010. LBNE Doc 3056.

[9] "LBNE Liquid Argon TPC Detector Case Study," tech. rep. LBNE-doc-3600.

[10] UA1 Collaboration. `http://library.web.cern.ch/library/archives/isad/isaua1.html`.

[11] A. Bernstein *et al.*, "Report on the Depth Requirements for a Massive Detector at Homestake (LBNE:DocDB-34)," 2009. arXiv:0907.4183 [hep-ex].

[12] "The LArSoft Collaboration." `https://plone4.fnal.gov:4430/P1/Main/wiki/LArSoft/LArSoft`.

[13] "A Proposal for a Detector 2 km Away from the T2K Neutrino Source," 2005. `http://www.phy.duke.edu/~cwalter/nusag-members/2km-proposal-05-05-30.pdf`.

[14] "A Large Liquid Argon Time Projection Chamber for Long-baseline Off-Axis Neutrino Oscillation Physics with the NuMI Beam," tech. rep., 2005. Submitted to the NuSAG committee; inspirehep.net FERMILAB-FN-0776-E.

[15] tech. rep. LBNE-doc-266-v1, LBNE-doc-3414-v2.

[16] tech. rep. LBNE-doc-5446.

[17] `http://icarus.lngs.infn.it/`.

[18] P. Adamson *et al.*, "Improved search for muon-neutrino to electron-neutrino oscillations in MINOS," *Phys. Rev. Lett.*, vol. 107, p. 181802.

[19] A. Ankowski *et al.*, "Measurement of through-going particle momentum by means of multiple scattering with the icarus t600 tpc.," *Eur. Phys. J.*, vol. C48, p. 667, 2006.

[20] W. A. Mann *et al.*, "Apparent multiple Δm^2_{32} in muon anti-neutrino and muon neutrino survival oscillations from non-standard interaction matter effect," *Phys. Rev. D.*, vol. 82, p. 113010, 2010.

[21] U. Kose, "Search for $\nu_\mu \to \nu_\tau$ oscillations in appearance mode in the OPERA experiment.." arXiv:1106.3871 [hep-ex], 2011.

[22] P. Adamson *et al.*, "Search for the disappearance of muon antineutrinos in the NuMI neutrino beam.," *Phys. Rev. D.*, vol. 84, p. 071103, 2011. arXiv:1108.1509 [hep-ex].

[23] J. Kopp arXiv:1010.3706.

[24] S. Davidson, C. Pena-Garay, N. Rius, and A. Santamaria hep-ph/0302093, 2003.

[25] M.C. Gonzalez-Garcia, and M. Maltoni *Phys. Rept.*, vol. 460, p. 1, 2008. arXiv:0704.1800 [hep-ph].

[26]

[27] H. Davoudiasl and others, "Long-Range Lepton Flavor Interactions and Neutrino Oscillations.," *Phys. Rev. D.*, vol. 84, p. 013009, 2011. arXiv:1102.5352 [hep-ph].

[28] P. Adamson and others, "Search for sterile neutrino mixing in the MINOS long baseline experiment," *Phys. Rev. D.*, vol. 81, p. 052004, 2010. arXiv:1001.0336 [hep-ex].

[29] A.Bueno *et al. JHEP*, vol. 0704, p. 041, 2007.

[30] M. Baldo-Ceolin *et al.*, "A new experimental limit on neutron - anti-neutron oscillations," *Z. Phys. C 63*, p. 409, 1994.

[31] K. Abe *et al.*, "The search for n-nbar oscillation in Super-Kamiokande I," arXiv:1109.4227 [hep-ex].

[32] T.Totani *et al.*, "Future detection of supernova neutrino burst and explosion mechanism," *Astrophys. J.*, vol. 496, p. 216, 1998.

[33] C. V. J. Gava, J. Kneller and G. C. McLaughlin *Phys. Rev. Lett.*, vol. 103, p. 071101, 2009. arXiv:0902.0317 [hep-ph].

[34] D. Barker *et al.*, "Muon-induced background study for an argon-based long baseline neutrino experiment," 2012. arXiv:1202.5000v1 [physics.ins-det].

[35] S. Coleman and S. Glashow *Phys. Rev. Lett.*, vol. B405, p. 249, 1997.

[36] F. Klinkhamer and G. Volovik *Intl. Jour. of Mod. Phys.*, vol. A20, p. 2795, 2005.

[37] D. Colladay and V. Kostelecky *Phys. Rev. D.*, p. 116002, 1998.

[38] Y. Grossman *et al. Phys. Rev. D.*, vol. 72, p. 125001, 2005.

[39] M. C. Gonzalez-Garcia *et al. Nucl. Phys. B*, vol. 573, p. 3, 2000.

[40] D. Kaplan *et al. Phys. Rev. Lett*, vol. 93, p. 091801, 2004.

[41] K. Abe *et al. Phys. Rev. D*, vol. 77, p. 052001, 2008.

[42] W. Wang. PhD thesis, 2007.

[43] G. Mitsuka, *Study of Non-Standard Neutrino Interactions with Atmospheric Neutrino Data in Super-Kamiokande*. PhD thesis, University of Tokyo, 2009.

[44] J. Conrad *et al.*, "Atmospheric tau neutrinos in a multi-kiloton liquid argon detector," 2010. arXiv:1008.2984/hep-ph.

[45] J. Altegoer *et al.*, "The NOMAD experiment at the CERN SPS," *Nucl. Instrum. Meth.*, vol. A404, p. 96, 1998.

[46] D. Casper, "The nuance neutrino physics simulation, and the future.," *Nucl.Phys.Proc.Suppl.*, vol. 112, p. 161, 2002.

[47] tech. rep. LBNE-doc-740.

[48] tech. rep. LBNE-doc-783.

[49] `http://www-e815.fnal.gov/`.